

Resource Management in Cooperative Multi-Agent Networks Through Self-Triggering

Domagoj Tolić, Vana Jeličić, and Vedran Bilas

Faculty of Electrical Engineering and Computing, University of Zagreb, Unska 3, 10000 Zagreb, Croatia
{domagoj.tolic, vana.jelicic, vedran.bilas}@fer.hr

Abstract

In this paper, our interest is to reduce requirements posed on communication, sensing, processing and energy resources in Multi-Agent Networks (MANs) without compromising objectives of the MANs. Consequently, the hardware expenses and energy consumption are driven down whilst MAN multitasking, such as inter-network collaboration, is facilitated. Scenarios, in which agents of one network need to achieve a common goal, call for the study of decentralized cooperative control schemes. In order to accomplish this goal in an uncertain and noisy setting and to detect changes in the communication topology, agents have to exchange information. Because each transmission and reception of information necessitates energy, communication should be induced only when the goal completion can no longer be guaranteed in order to prolong the MAN mission. To that end, we devise an information exchange mechanism which draws upon ideas of self-triggered communication. The proposed mechanism is inspected both theoretically and experimentally (employing off-the-shelf wireless sensor platforms) for performance vs. lifetime trade-offs using a single-integrator consensus case study. Our mechanism is applicable to heterogeneous agents with exogenous disturbances (or modeling uncertainties), to switching communication topologies and to both initial-condition-dependent and initial-condition-independent long-term cooperative behaviors. The investigated stability notions include \mathcal{L}_p -stability and Input-to-State Stability (with respect to a set).

1 Introduction

The emergence of new technologies provides networks of increasingly accomplished agents. Such agents may be mobile and may possess significant processing, sensing, communication as well as memory and energy storage capabilities (refer to Figure 1). At the same time, aspirations to satisfy evergrowing demands of the industrial and civil sectors bring about novel engineering paradigms such as Cyber-Physical Systems [1] and Internet of Things [2]. The essence of these paradigms is fairly similar – to

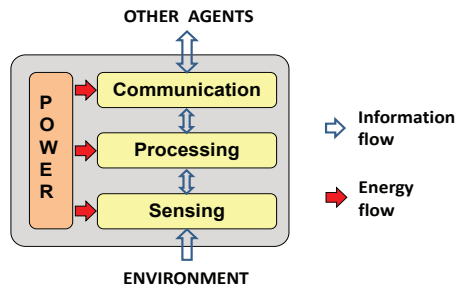


Figure 1: Block scheme of an agent indicating information and energy flows.

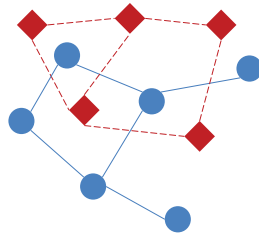


Figure 2: Two decentralized co-located MANs.

extend even further the concepts of heterogeneity, safety, decentralization, scalability, reconfigurability, and robustness of Multi-Agent Networks (MANs) by laying more burden on the agents. Everyday examples of MANs are cooperative multi-robot systems [3] and Wireless Sensor Networks (WSNs) [4].

According to [1, 2, 5], we are heading towards densely deployed MANs that coexist side by side sharing the same physical environment as illustrated in Figure 2. In order to realize the full potential of MANs, one typically allows each agent of a network to interact with any agent of neighboring networks. In other words, the existence of specialized agents (e.g., gateways) is no longer required to achieve inter-network collaboration. Neighboring MANs may need to share information (e.g., measurements, intentions) as well as resources and services (e.g., storage space, energy supplies, processing power, Internet or routing services). However, this interaction must not compromise objectives of each individual network. Commonly investigated objectives of stand-alone networks are consensus attainment [3, 6, 7] and output synchronization [8–10].

Agents usually have limited and costly resources at their disposal which renders agent resource management of critical importance. Recently, several authors have proposed an avenue towards agent resource management by means of decentralized *event-triggered* and *self-triggered* control/sensing/communication schemes (refer to [8, 9, 11] and [6, 7, 10, 12, 13], respectively). In event-triggered schemes, one defines a desired performance and a transmission of up-to-date information is induced when an event representing the unwanted performance occurs. In this paper, the desired performance is closed-loop stability. In self-triggered approaches, currently available information are used to compute the next transmission instant, i.e., to *predict* the occurrence of the triggering event. Therefore, self-triggering

enables agents to predict time intervals of idleness over which energy conservation modes can be activated [14–16]. Alternatively, agents can freely engage in other activities (e.g., inter-network collaboration) prior to the (pre)computed transmission instant. As a caveat, the performance of event- and self-triggered control schemes is more susceptible to disturbances, modeling uncertainties and noise due to longer open-loop-control intervals [17]. While [17] and the references therein bring theoretical studies of performance vs. resource consumption trade-offs for plant-controller control problems, the work presented herein investigates theoretically and experimentally these trade-offs for MANs. To the best of our knowledge, these trade-offs for MANs are yet to be addressed both theoretically and experimentally.

Since a good deal of works regarding event- and self-triggering are still being published, it is clear that this area has not matured yet and further research endeavors are vital. In fact, most of the proposed methodologies are applicable to a rather specific application-dependent setting (e.g., specific agent and controller dynamics as well as specific topology and inter-agent coupling), which often hinders equitable comparisons between methodologies and impedes their transferability to a different setting. Thus, generalizing and unifying frameworks are needful. To that end, we devise a unifying framework for general heterogeneous agents with (possibly dynamic and output-feedback) local controllers in the presence of exogenous disturbances (or modeling uncertainties) and switching topologies. We point out that, save for [8], all aforementioned works consider state-feedback controllers. The unifying feature of our framework is manifested in the fact that both initial-condition-dependent and initial-condition-independent long-term behaviors of MANs can be analyzed. For example, initial-condition-dependent long-term behaviors are investigated in [6–8, 10] while initial-condition-independent long-term behaviors are addressed in [9, 11–13].

The principal requirement in our framework is \mathcal{L}_p -stability (with respect to a set) of the closed-loop system. In other words, we do not impose specific requirements on the agent and controller dynamics per se nor on the underlying communication topology. Basically, when given local controllers do not yield the closed-loop system \mathcal{L}_p -stable (with respect to a set), one can seek for another topology or design alternative controllers. In this regard, our framework is akin to [12] and [11]. Nevertheless, the requirements in [12] and [11] are imposed locally on each agent (i.e., \mathcal{L}_p -stability and Input-to-State Stability properties, respectively) and on agent interactions (i.e., weak coupling). In addition, self-triggered counterparts of [11, 12] are still to be devised. Furthermore, [8] requires proportional controllers and passive agents, which in turn implies that the number of inputs equals the number of outputs for all agents, while [6] investigates single-integrator agents with proportional control laws. The authors in [9] impose the Hurwitz condition on local dynamics (rather than on the closed-loop

dynamics) and the diagonal dominant matrix structure on the nominal closed-loop dynamics. In [7], the authors tailor several ternary controllers for self-triggered practical consensus of single-integrator agents and show that those controllers possess some desirable robustness features. As opposed to [7], our methodology, as well as the methodologies in [8, 11, 12], aims at devising triggering conditions for a variety of existing control schemes that are designed on the premise of continuous information flows. As far as communication topologies are concerned, only [8] considers time-varying topologies (though balanced ones). Furthermore, [6] and [7] consider undirected fixed topologies. On the other hand, our framework encompasses directed switching topologies. It is worth mentioning that the approaches in [6] and [12] are not Zeno free. Lastly, unlike [6–9, 11], our work is able to consider external disturbances (or modeling uncertainties).

The main contributions of this work are fourfold: a) the design of a self-triggered communication mechanism for both initial-condition-dependent and initial-condition-independent cooperative tasks in the presence of exogenous disturbances; b) a theoretical and experimental investigation of the performance vs. lifetime trade-offs for the single-integrator consensus problem; c) an experimental conservativeness analysis of theoretically obtained upper bounds on stabilizing transmission intervals; and d) a detailed exposition of implementation issues for the developed self-triggered communication mechanism. Let us point out that the theory presented herein builds upon [10, 13] and detailed proofs of the presented results are provided. Note that [13] and [10] contain no proofs. In addition, the experimental results presented herein validate the theoretical/simulation results of [10, 17].

The remainder of the paper is organized as follows. Section 2 presents the notation and terminology used throughout this paper. Section 3 formulates the self-triggered information exchange problem for MANs comprised of heterogeneous linear systems. Consequently, we state problems related to feasibility of self-triggered mechanisms as well as to the pertaining theoretical and experimental MAN performance vs. lifetime analyses. Our self-triggered mechanism is devised in Section 4. Theoretical performance vs. lifetime trade-offs and experimental results for a single-integrator consensus case study are in Section 5. Conclusions and future challenges are found in Section 6. Graph theory concepts, several technical results and proofs are included in the Appendix.

2 Preliminaries

2.1 Notation and Terminology

In order to shorten the notation, we use $(x, y) := [x^\top \quad y^\top]^\top$. The dimension of a vector x is denoted n_x . In this paper, $\|\cdot\|$ refers to the Euclidean norm of a vector. If the argument of $\|\cdot\|$ is a matrix,

then it denotes the induced matrix 2-norm. The kernel (or null space) of a matrix A is denoted $\text{Ker}(A)$. The dimension of $\text{Ker}(A)$ is denoted $\mathcal{G}(A)$ and equals the geometric multiplicity of the zero eigenvalue [18, Definition B.14]. The algebraic multiplicity of the zero eigenvalue is denoted $\mathcal{A}(A)$.

Given $x \in \mathbb{R}^n$, we define

$$\bar{x} = (|x_1|, |x_2|, \dots, |x_n|),$$

where $|\cdot|$ denotes the absolute value function. When the argument of $|\cdot|$ is a set, then it denotes the cardinality of the set. Given $x = (x_1, x_2, \dots, x_n)$ and $y = (y_1, y_2, \dots, y_n) \in \mathbb{R}^n$, the partial order \preceq is given as

$$x \preceq y \iff x_i \leq y_i \quad \forall i \in \{1, \dots, n\}.$$

The element-wise product of the i^{th} and j^{th} column of a matrix A is denoted $A(i).A(j)$ while the n^{th} -dimensional vector of all entries 0 (respectively, 1) is denoted $\mathbf{0}_n$ (respectively, $\mathbf{1}_n$). Likewise, the $n \times n$ identity matrix is denoted \mathbf{I}_n , while the $n \times m$ matrix with all zero entries is $\mathbf{0}_{n \times m}$. Let \mathbb{R}_+^n denote the nonnegative orthant. The set \mathcal{A}_n^+ denotes the subset of all $n \times n$ matrices that are symmetric and have nonnegative entries.

For the sake of brevity, we write ‘‘w.r.t.’’ instead of ‘‘with respect to’’ throughout the paper. We use

$$\|f[a, b]\|_{p, \mathcal{B}} := \left(\int_{[a, b]} \|f(s)\|_{\mathcal{B}}^p ds \right)^{1/p}, \quad (1)$$

where $\|f(s)\|_{\mathcal{B}} := \inf_{b \in \mathcal{B}} \|f(s) - b\|$, to denote the \mathcal{L}_p -norm w.r.t. a set $\mathcal{B} \subset \mathbb{R}^n$ of a Lebesgue measurable function $f : \mathbb{R} \rightarrow \mathbb{R}^n$ restricted to the interval $[a, b] \subset \mathbb{R}$. Lastly, when $\mathcal{B} = \mathbf{0}_n$, we write $\|f[a, b]\|_p$ since this represents the standard \mathcal{L}_p -norm. The dominant growth rate of a function $f(x) : \mathbb{R}^{n_x} \rightarrow \mathbb{R}$ is denoted $O(f)$. Since this dominant growth rate is in line with the big O notation, we adopt the letter O .

2.2 Stability Notions

Consider a nonlinear impulsive (or hybrid) system

$$\Sigma \left\{ \begin{array}{l} \dot{x} = f(x, \omega) \\ y = g(x, \omega) \end{array} \right\} t \in \bigcup_{i \in \mathbb{N}_0} [t_i, t_{i+1}), \quad (2)$$

$$x(t^+) = h(x(t)) \quad t \in \mathcal{T},$$

where $x \in \mathbb{R}^{n_x}$ denotes the state, $\omega \in \mathbb{R}^{n_\omega}$ reflects the external disturbance (or modeling uncertainties), and $y \in \mathbb{R}^{n_y}$ denotes the output of the system. We assume enough regularity on f and h to guarantee existence of the solutions given by right-continuous functions $t \mapsto x(t)$ on $[t_0, \infty)$ starting from x_0 at $t = t_0$. Jumps of the state x (or impulses) occur at each $t \in \mathcal{T} := \{t_i : i \in \mathbb{N}\}$. The value of the state after the jump is given by $x(t^+) = \lim_{t' \searrow t} x(t')$ for each $t \in \mathcal{T}$. For a comprehensive discussion of impulsive systems, refer to [19].

In the following definitions, we use the set

$$\mathcal{B}_y := \{y \in \mathbb{R}^{n_y} \mid \exists b \in \mathcal{B} \text{ such that } y = g(b, \mathbf{0}_{n_\omega})\}, \quad (3)$$

where $\mathcal{B} \subseteq \mathbb{R}^{n_x}$.

Definition 1. (*Uniform Global Exponential Stability w.r.t. a set*) For $\omega \equiv \mathbf{0}_{n_\omega}$, the system Σ is *Uniformly Globally Exponentially Stable (UGES) w.r.t. a set \mathcal{B}* if there exist $k, l > 0$ such that $\|x(t)\|_{\mathcal{B}} \leq k \exp(-l(t - t_0)) \|x(t_0)\|_{\mathcal{B}}$ for all $t \geq t_0$ and for any $x(t_0)$.

Definition 2. (*Input-to-State Stability w.r.t. a set*) The system Σ is *Input-to-State Stable (ISS) w.r.t. a set \mathcal{B}* if there exist a class- \mathcal{KL} function β and a class- \mathcal{K}_∞ function γ such that, for any $x(t_0)$ and every input ω , the corresponding solution $x(t)$ satisfies $\|x(t)\|_{\mathcal{B}} \leq \beta(\|x(t_0)\|_{\mathcal{B}}, t - t_0) + \gamma(\|\omega[t_0, t]\|_\infty)$.

Definition 3. (*\mathcal{L}_p -stability w.r.t. a set*) Let $p \in [1, \infty]$. The system Σ is *\mathcal{L}_p -stable from ω to y w.r.t. a set \mathcal{B} with gain $\gamma \geq 0$* if there exists $K \geq 0$ such that $\|y[t_0, t]\|_{p, \mathcal{B}_y} \leq K \|x(t_0)\|_{\mathcal{B}} + \gamma \|\omega[t_0, t]\|_p$ for any $t \geq t_0$, $x(t_0)$ and ω .

Definition 4. (*\mathcal{L}_p -detectability w.r.t. a set*) Let $p \in [1, \infty]$. The state x of Σ is *\mathcal{L}_p -detectable from (ω, y) to x w.r.t. a set \mathcal{B} with gain $\gamma_d \geq 0$* if there exists $K_d \geq 0$ such that $\|x[t_0, t]\|_{p, \mathcal{B}} \leq K_d \|x(t_0)\|_{\mathcal{B}} + \gamma_d \|y[t_0, t]\|_{p, \mathcal{B}_y} + \gamma_d \|\omega[t_0, t]\|_p$ for any $t \geq t_0$, $x(t_0)$ and ω .

Definitions 1 and 2 are motivated by [20] and [21], while Definitions 3 and 4 are motivated by [22]. Notice that K , γ , K_d and γ_d in Definitions 3 and 4 are not unique.

2.3 Switched Systems and Average Dwell-Time

Consider a family of systems (2) indexed by the parameter ρ taking values in a set $\mathcal{P} = \{1, 2, \dots, m\}$. Let us define a right-continuous and piecewise constant function $\sigma : [t_0, \infty) \rightarrow \mathcal{P}$ called a *switching signal* [23]. The role of σ is to specify which system is active at any time $t \geq t_0$. The resulting switched

system investigated herein is given by

$$\Sigma_\sigma \left\{ \begin{array}{l} \dot{x} = f_\sigma(x, \omega) \\ y = g(x, \omega) \end{array} \right\} t \in \bigcup_{i \in \mathbb{N}_0} [t_i, t_{i+1}), \quad (4)$$

$$x(t^+) = h_\sigma(x(t)) \quad t \in \mathcal{T}.$$

For each switching signal σ and each $t \geq t_0$, let $N_\sigma(t, t_0)$ denote the number of discontinuities, called *switching times*, of σ on the open interval (t_0, t) . We say that σ has *average dwell-time* τ_a if there exist $N_0, \tau_a > 0$ such that

$$N_\sigma(t, t_0) \leq N_0 + \frac{t - t_0}{\tau_a} \quad (5)$$

for every $t \geq t_0$. For a comprehensive discussion, refer to [23] and [24]. In this paper, different values of σ correspond to different topologies L , while state jump instants t_i 's indicate time instants at which an exchange of information takes place.

Notice that our definitions of impulsive and switched systems do not explicitly rule out accumulations of jumping and switching instants in finite time as it is typically done in the literature (e.g., [23], [24] [25], [3, Chapter 2]). A priori exclusions of these phenomena are not in the essence of self-triggered communication. In fact, valid self-triggered communication policies must guarantee that communication instants do not accumulate in finite time which is known as Zeno behavior (refer to Remark 3). Consequently, self-triggering eliminates the problem of arbitrary fast switching because changes in the communication topology are irrelevant while information are not being exchanged.

3 Problem Statement

Under the premise of continuous information exchange between neighboring agents, the closed-loop dynamics of a large class of MAN control problems can be written as the following switched linear system:

$$\begin{aligned} \dot{x} &= A_\sigma^{\text{cl}} x + \omega, \\ y &= C^{\text{cl}} x, \end{aligned} \quad (6)$$

where x, y and ω are stack vectors comprised of (possibly translated) agents' states, outputs and exogenous disturbances (or modeling uncertainties), respectively. In other words, when N agents are considered, it follows that $x := (\xi_1, \xi_2, \dots, \xi_N) - \xi_\sigma^{\text{p}}$, $y := (\zeta_1, \zeta_2, \dots, \zeta_N) - \zeta_\sigma^{\text{p}}$ and $\omega := (\omega_1, \omega_2, \dots, \omega_N)$,

where ξ_i , ζ_i and ω_i are the i^{th} agent state, output and exogenous disturbance, respectively. Because of the translation of $(\xi_1, \xi_2, \dots, \xi_N)$ by a particular solution ξ_σ^{p} , the equilibrium manifold of the closed-loop dynamics includes the origin when $\omega \equiv \mathbf{0}_{n_\omega}$. The associated output is ζ_σ^{p} . Appendix 6.2 delineates steps relating (6) with linear heterogeneous agents and control laws commonly found in the literature. Notice that, for a finite number of agents N , there can be at most 2^{N^2-N} different topologies (i.e., individual systems constituting the switched system) as self-loops are not allowed. Accordingly, $|\mathcal{P}| = m$, where $m \leq 2^{N^2-N}$. Relevant graph theory concepts are provided in Appendix 6.1.

Assuming that all individual systems in (6) are characterized by the same equilibrium manifold, let us define

$$\mathcal{B} := \text{Ker}(A_\rho^{\text{cl}}) = \text{Ker}(A_\varrho^{\text{cl}}) \quad \forall \rho, \varrho \in \mathcal{P}.$$

Apparently, \mathcal{B} represents the set of equilibrium points when $\omega \equiv \mathbf{0}_{n_\omega}$. Consequently,

$$\mathcal{B}_y := \{y \in \mathbb{R}^{n_y} \mid x \in \mathcal{B} \text{ such that } y = C^{\text{cl}}x\}.$$

Assumption 1. For each $\rho \in \mathcal{P}$, all eigenvalues of A_ρ^{cl} have nonpositive real parts. In addition, the eigenvalues with zero real part are located in the origin and $\mathcal{A}(A_\rho^{\text{cl}}) = \mathcal{G}(A_\rho^{\text{cl}})$ for each $\rho \in \mathcal{P}$.

Remark 1. In case $\mathcal{B} \neq \mathbf{0}_{n_x}$, i.e., $\mathcal{A}(A_\rho^{\text{cl}}) = \mathcal{G}(A_\rho^{\text{cl}}) \neq 0$ for each $\rho \in \mathcal{P}$, the MAN long-term behavior depends on the agents' initial conditions. Basically, $\text{Ker}(A_\rho^{\text{cl}})$ is nontrivial, spanned by the eigenvectors corresponding to the zero eigenvalue and represents the equilibrium manifold. Such matrices are typically found in coordinated tasks that seek primarily for an agreement while the actual value of the agreement/consensus point depends on the agents initial conditions. When $\mathcal{A}(A_\rho^{\text{cl}}) = \mathcal{G}(A_\rho^{\text{cl}}) = 0$, $\rho \in \mathcal{P}$, then A_ρ^{cl} is Hurwitz and the MAN long-term behavior is independent of the agents' initial conditions as there is merely one attractor – the sole equilibrium point.

Definition 5. Suppose we have a closed-loop system given by (6). We say that the MAN achieves its objective if $y \rightarrow \mathcal{B}_y$ as $t \rightarrow \infty$.

Remark 2. The above definition includes both output and state synchronization/consensus problems (consult [8, 13] and [6, 7, 9–12], respectively). The latter is characterized by $C^{\text{cl}} = \mathbf{I}_{n_x}$.

Recall that (6) is obtained on the premise of continuous information exchange among neighbors. However, continuous information flows in real-life applications are often not achievable because:

- (i) *digital technology might be employed:* Every agent operation takes a certain amount of time for

completion. Consequently, the hardware-specific *minimal time* to broadcast/receive a packet by a wireless radio transceiver determines *maximal frequency* of communication.

- (ii) *an agent cannot broadcast and receive simultaneously*: Unless there are two parallel communication channels (one only for transmitting and one only for receiving), a wireless device can either broadcast or receive at a particular moment. Since a double communication channel yields a big overhead in terms of complexity and energy consumption of devices, it is not desirable in most applications.
- (iii) *a radio transceiver cannot receive messages when inactive*: In order for an agent radio to receive a message, it has to *listen* the communication medium and switch to the *active* operation mode. Because the power consumption of the radio while actually receiving and while merely listening is practically the same (see [14–16] and Section 5), it is desirable to replace portions of listening intervals with idle intervals when no incoming information is expected.
- (iv) *message collision*: When several messages are being received at a receiver’s end simultaneously, the associated data are lost. To avoid such collisions, TDMA (Time Division Multiple Access) approaches, where each agent has a pre-scheduled time slot to access the communication medium, are often used. In this case, synchronization of the agent clocks is crucial [26] and often achieved via consensus-seeking strategies.

Nevertheless, in spite of all these limitations, MAN cooperation is still being achieved in realistic settings. This observation indicates that there is some built-in robustness of the closed-loop dynamics (6) with respect to the intermittent information exchange. By thriving on this built-in robustness, self-triggering extends agents’ lifetime and allows the agents to engage in inter-network activities. However, as pointed out in the introductory section, self-triggering consensus degrades network performance due to greater susceptibility to modeling uncertainties and exogenous disturbances [17].

Problem 1. *Modify the closed-loop dynamics (6) such that the above hardware limitations are taken into account and design a self-triggered data exchange mechanism.*

Problem 2. *Theoretically investigate MAN performance vs. lifetime trade-offs when the designed self-triggered mechanism is employed.*

Problem 3. *Experimentally validate the obtained theoretical results.*

4 Methodology

In order to account for intermittent data exchange, the closed-loop system (6) can be modified as follows:

$$\dot{x} = A_\sigma^{\text{cl}}x + B_\sigma^{\text{cl}}e + \omega, \quad (7)$$

where B_σ^{cl} is a matrix of appropriate dimensions and e is an auxiliary error signal with the following dynamics

$$\dot{e} = -C^{\text{cl}}\dot{x}. \quad (8)$$

Further details regarding B_σ^{cl} and e are not needed to follow the subsequent exposition. Nevertheless, the interested reader is referred to the Appendix 6.3 where B_σ^{cl} and e are constructed for common cooperative control problems.

From (7), we infer that the underlying communication topology captured in $\sigma(t)$, i.e., in the graph Laplacian matrix L_σ , plays an instrumental role in cooperative control. Consequently, agents need to discover the underlying communication topology in a decentralized manner. To that end, we advocate the approach from [27] due to its finite-time-convergence property and applicability to directed graphs. According to [27], the following assumption needs to be placed on the communication topology.

Assumption 2. *All unidirectional links have an inclusive cycle.*

After discovering a certain L_ρ , where $\rho \in \mathcal{P}$, agents utilize that knowledge to synchronize broadcasting/receiving instants in order to avoid lost packages due to (ii), (iii) and (iv) of Section 3. Namely, only those agents that have no common receivers and are not receivers themselves at a particular time instant are allowed to broadcast their states. By grouping such agents via Algorithm 1 into subsets \mathcal{P}_ρ^i , an agent partition is obtained. The input to the algorithm is L_ρ and the outputs are subsets \mathcal{P}_ρ^i . The number of nonempty \mathcal{P}_ρ^i 's is $T_\rho \leq N$ and empty \mathcal{P}_ρ^i 's are pruned. Figure 3 illustrates the partition obtained for

$$L_\rho = \begin{bmatrix} 2 & -1 & 0 & -1 & 0 \\ 0 & 1 & -1 & 0 & 0 \\ 0 & 0 & 1 & 0 & -1 \\ -1 & -1 & 0 & 2 & 0 \\ 0 & 0 & -1 & -1 & 2 \end{bmatrix}. \quad (9)$$

Algorithm 1 The algorithm developed for graph partitioning. Taking L_ρ , where $\rho \in \mathcal{P}$, as the input, the algorithm outputs a partition $\{\mathcal{P}_\rho^1, \dots, \mathcal{P}_\rho^N\}$.

```

 $\mathcal{P}_\rho^i \leftarrow \{\emptyset\}$  for all  $i \in \{1, \dots, N\}$ ;  $k \leftarrow 0$ 
for  $i = 1$  to  $N$  do
  if  $i \notin \mathcal{P}_\rho^m$  for every  $m \in \{1, \dots, N\}$  then
     $k \leftarrow k + 1$ 
     $\mathcal{P}_\rho^k \leftarrow \mathcal{P}_\rho^k \cup \{i\}$ 
    for  $j = i + 1$  to  $N$  do
      if  $L_\rho(i).L_\rho(j) = \mathbf{0}_N$  for all  $i \in \mathcal{P}_\rho^k$  then
         $\mathcal{P}_\rho^k \leftarrow \mathcal{P}_\rho^k \cup \{j\}$ 
      end if
    end for
  end if
end for
end if
end for

```

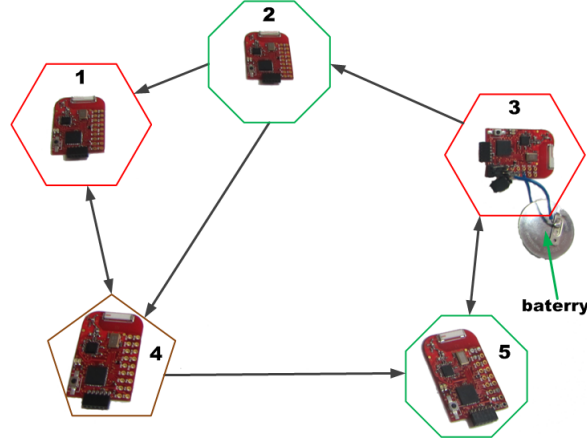


Figure 3: The graph partition $\mathcal{P}_\rho^1 = \{1, 3\}$, $\mathcal{P}_\rho^2 = \{2, 5\}$ and $\mathcal{P}_\rho^3 = \{4\}$ obtained via Algorithm 1. Accordingly, $T_\rho = 3$. In order not to clutter this figure with a battery for each node, only Node 3 is connected to a battery.

4.1 Designing Broadcasting Instants

Let us now design stabilizing broadcasting instants for each \mathcal{P}_ρ^i . For simplicity, let us consider the following TDMA scheduling protocol illustrated in Figure 4.

Protocol 1. *The agents from $\mathcal{P}_\rho^{[(i+1) \bmod N]+1}$ broadcast their outputs τ_ρ seconds after the agents from $\mathcal{P}_\rho^{[i \bmod N]+1}$ have broadcast their outputs, where $a \bmod b$ denotes the remainder of the division of a by b for $a, b \in \mathbb{N}$.*

The impact of broadcasting agents' outputs is as follows:

Property 1. *If the i^{th} agent broadcasts at time t , the corresponding components of e reset to zero while other components remain unchanged, i.e.,*

$$\left. \begin{aligned} e_{(i-1)n_\zeta+1}^+(t) &= \dots = e_{in_\zeta}^+(t) = 0, \\ e_j^+(t) &= e_j(t), \end{aligned} \right\} \quad (10)$$

for all $j \in \{1, \dots, Nn_\zeta\} \setminus \{(i-1)n_\zeta+1, \dots, in_\zeta\}$, where the set difference is denoted \setminus .

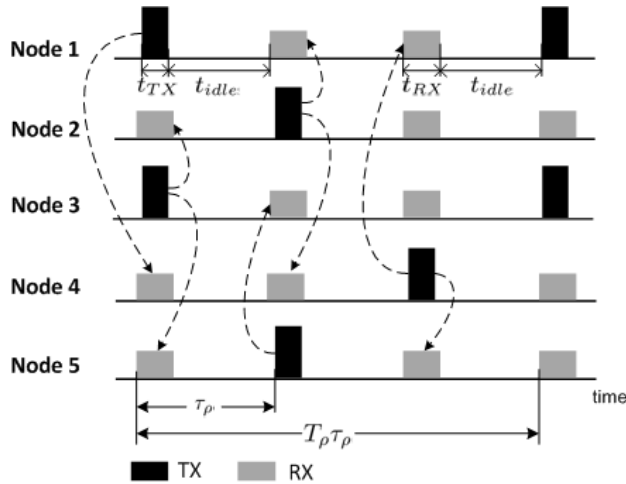


Figure 4: An illustration of the considered TDMA scheduling for the partition depicted in Figure 3. The abbreviation TX stands for *transmission* while RX stands for *reception*. Apparently, our TDMA scheduling prevents limitations (i)-(iv) from Section 3 for a sufficiently large τ_ρ , i.e., $\tau_\rho \geq \max\{t_{TX}, t_{RX}\}$ for each $\rho \in \mathcal{P}$. On the other hand, τ_ρ has to be sufficiently small in order to preserve closed-loop stability.

Due to the extensions of [22] reported in [28], our framework is applicable to the larger class of *uniformly persistently exciting scheduling protocols* [22] and not merely to Protocol 1. However, we do not pursue that direction herein in order not to obfuscate the main points of the present paper.

As can be inferred from Protocol 1, agents know when they should “hear” from their neighbors, which is a prominent feature of self-triggering. When an agent does not “hear” from a neighbor in the precomputed time interval, that agent induces the topology discovery algorithm [27] in order to keep track of changes in the communication topology. Upon discovering a new topology, an up-to-date partition is obtained via Algorithm 1, the corresponding TDMA scheduling commences, and so on. Consequently, τ_ρ from Protocol 1 adapts to the new topology in order to preserve MAN stability. As a result, one could label our self-triggered control scheme as *topology-triggering*. However, we do not insist on the term topology-triggering in order not to inundate the area with excessive terminology. For instance, [6] and [7] devise state-triggering, [28] designs input-output-triggering while [29] develops team-triggering.

We are still left to compute values of τ_σ that stabilize the closed-loop system (7)-(8) with intermittent data exchange. To that end, let us interconnect dynamics (7) and (8) and employ the small-gain theorem [20]. First, we upper bound the output error dynamics (8) for a fixed topology, i.e., $\sigma(t) \equiv \rho$ for some $\rho \in \mathcal{P}$, as follows:

$$\bar{e} = \overline{-C^{\text{cl}}(A_\rho^{\text{cl}}x + B_\rho^{\text{cl}}e + \omega)} \preceq A_\rho^* \bar{e} + \tilde{y}_\rho(x, \omega), \quad (11)$$

where

$$A_\rho^* = [a_{ij}^*] := \max\{|c_{ij}^*|, |c_{ji}^*|\}, \quad (12)$$

$$\tilde{y}_\rho(x, \omega) := \overline{-C^{\text{cl}}(A_\rho^{\text{cl}}x + \omega)}. \quad (13)$$

In (12), we use $-C^{\text{cl}}B_\rho^{\text{cl}} = [c_{ij}^*]$. Notice that $A_\rho^* \in \mathcal{A}_{n_e}^+$ and $\tilde{y}_\rho : \mathbb{R}^{n_x} \times \mathbb{R}^{n_\omega} \rightarrow \mathbb{R}_+^{n_e}$ is a continuous function. With this choice of A_ρ^* and \tilde{y}_ρ , the upper bound (11) holds for all $(x, e, \omega) \in \mathbb{R}^{n_x} \times \mathbb{R}^{n_e} \times \mathbb{R}^{n_\omega}$ and all $t \in \mathbb{R}$.

Theorem 1. *Suppose that Protocol 1 is implemented and $\sigma(t) \equiv \rho$, where $\rho \in \mathcal{P}$. In addition, suppose that $\tau_\rho \in (0, \tau_\rho^*)$, where $\tau_\rho^* := \frac{\ln(2)}{\|A_\rho^*\|T_\rho}$. Then, the error system (8) is \mathcal{L}_p -stable from \tilde{y}_ρ , given by (13), to e for any $p \in [1, \infty]$ with gain*

$$\gamma_\rho^e = \frac{T_\rho \exp(\|A_\rho^*\|(T_\rho - 1)\tau_\rho)(\exp(\|A_\rho^*\|\tau_\rho) - 1)}{\|A_\rho^*\|(2 - \exp(\|A_\rho^*\|T_\rho\tau_\rho))}, \quad (14)$$

and constant

$$K_\rho^e = \frac{1}{2 - \exp(\|A_\rho^*\|T_\rho\tau_\rho)} \left(\frac{\exp(p\|A_\rho^*\|T_\rho\tau_\rho) - 1}{p\|A_\rho^*\|} \right)^{\frac{1}{p}}. \quad (15)$$

Proof. This result is obtained following the proof of [22, Theorem 5.1]. However, the assumptions of [22, Theorem 5.1] require A_ρ^* both to be positive semidefinite and to belong to $\mathcal{A}_{n_e}^+$. Positive semidefiniteness of A_ρ^* , together with the requirement that $A_\rho^* \in \mathcal{A}_{n_e}^+$, is imposed in [22] to establish equality $\|\exp(A_\rho^*)\| = \exp(\|A_\rho^*\|)$. Using [28, Lemma 1 & 2], the work in [28] shows that equality $\|\exp(A_\rho^*)\| = \exp(\|A_\rho^*\|)$ holds for matrices in $\mathcal{A}_{n_e}^+$. In other words, the requirement on A_ρ^* to be positive semidefinite is redundant. \square

Next, take (e, ω) to be the input and \tilde{y}_ρ , given by (13), to be the output of the dynamics (7). For future reference, this system is termed *nominal system*. Due to Assumption 1, [10, Theorem 1] yields \mathcal{L}_p -stability w.r.t \mathcal{B} of the system (7) with input (ω, e) and any output \dot{y}_ρ linear in x and ω . In addition, [10, Theorem 1] provides expressions for an associated constant and \mathcal{L}_p -gain. The following proposition shows that one can employ [10, Theorem 1] to infer \mathcal{L}_p -stability of (7) for the (nonlinear) output \tilde{y}_ρ given by (13).

Proposition 1. *Suppose that the system (7) with input (ω, e) and (linear) output $\dot{y}_\rho := -C^{\text{cl}}(A_\rho^{\text{cl}}x + \omega)$ is \mathcal{L}_p -stable w.r.t \mathcal{B} with some constant K_ρ and gain γ_ρ . Then, the system (7) with input (ω, e) and (nonlinear) output \tilde{y}_ρ , given by (13), is \mathcal{L}_p -stable w.r.t \mathcal{B} with the same constant K_ρ and gain γ_ρ .*

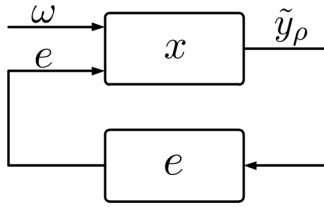


Figure 5: Interconnection of the nominal and the error dynamics.

Proof. Refer to Appendix 6.4. □

Apparently, systems (7) and (8) are interconnected according to Figure 5. We point out that \tilde{y}_ρ is an auxiliary signal used to interconnect (7) and (8), but does not exist physically. According to the small-gain theorem, the open loop gain $\gamma_\rho \gamma_\rho^e$ must be strictly less than unity in order for this interconnection to be \mathcal{L}_p -stable from ω to (\tilde{y}_ρ, e) w.r.t. $(\mathcal{B}_y, \mathbf{0}_{n_e})$ and, due to \mathcal{L}_p -detectability of the nominal system (see the proof of Theorem 2 for more), \mathcal{L}_p -stable from ω to (x, e) w.r.t. $(\mathcal{B}, \mathbf{0}_{n_e})$.

Theorem 2. *If the interbroadcasting interval τ_ρ in (14) is such that $\gamma_\rho \gamma_\rho^e < 1$, then the MAN objective in the sense of Definition 5 is \mathcal{L}_p -stable from ω to (x, e) w.r.t. $(\mathcal{B}, \mathbf{0}_{n_e})$ for given $p \in [1, \infty]$.*

Proof. Provided in Appendix 6.5. □

Remark 3. *Notice that $\gamma_\rho^e(\tau_\rho)$ in (14) is a monotonically increasing function of $\tau_\rho \in [0, \tau_\rho^*)$. In addition, notice that $\gamma_\rho^e(0) = 0$. Due to [10, Theorem 1], we know that $\gamma_\rho < \infty$. Since our goal is to design τ_ρ such that $\gamma_\rho \gamma_\rho^e(\tau_\rho) < 1$, we first find τ'_ρ such that $\gamma_\rho \gamma_\rho^e(\tau'_\rho) = 1$, and then compute $\tau_\rho = \kappa \tau'_\rho$, where $\kappa \in (0, 1)$. Due to monotonicity of $\gamma_\rho^e(\tau_\rho)$, the obtained τ'_ρ is strictly positive; hence, $\tau_\rho = \kappa \tau'_\rho$ is strictly positive. Consequently, the unwanted Zeno behavior [25] is avoided. In other words, our approach does not yield continuous feedback that is impossible to implement in digital technology. Since we are interested in obtaining the interbroadcasting interval τ_ρ as large as possible, we choose κ as great as possible (e.g., $\kappa = 0.999$).*

Remark 4. *Let us consider the case of lossy communication channels. If there is an upper bound on the maximum number of successive dropouts in the wireless network, say $M \in \mathbb{N}$, simply use $\tau_\rho / (M + 1)$ as the interbroadcasting interval and modify Protocol 1 so that each partition broadcasts consecutively $M + 1$ times in order for Theorem 2 to hold.*

4.2 Switching Communication Topologies

Before proceeding further, we point out that scenarios with $\mathcal{B} = \mathbf{0}_{n_x}$ are less involved and do not entail all the steps delineated below (when compared to scenarios with $\mathcal{B} \neq \mathbf{0}_{n_x}$). Essentially, scenarios with $\mathcal{B} = \mathbf{0}_{n_x}$ boil down to [13, Section V].

4.2.1 Switching without Disturbances

The previous subsection establishes \mathcal{L}_p -stability of the interconnection in Figure 5. In what follows, we demonstrate that this interconnection is UGES w.r.t. $(\mathcal{B}, \mathbf{0}_{n_e})$ when $\omega \equiv \mathbf{0}_{n_\omega}$. To that end, we introduce the following substitution (i.e., change of coordinates)

$$z = S_\rho x,$$

where S_ρ is an invertible matrix with real entries that transforms A_ρ^{cl} into the Real Jordan Form (refer to [10, Section IV.A] for more details). According to [10, Section IV.B], \mathcal{B} is spanned by the last \mathcal{A} columns of S_ρ^{-1} . In addition, the complementary space of \mathcal{B} , denoted \mathcal{B}^c , is spanned by the first $n_x - \mathcal{A}$ columns of S_ρ^{-1} . Having that said, it is convenient to label the first $n_x - \mathcal{A}$ entries of z as z_r and the last \mathcal{A} entries of z as z_q , i.e.,

$$z := (z_r, z_q).$$

As a result, we can write

$$x = S_\rho^{-1} z = S_\rho^{-1} ((z_r, \mathbf{0}_{\mathcal{A}}) + (\mathbf{0}_{n_x - \mathcal{A}}, z_q)).$$

Thus,

$$\|x\|_{\mathcal{B}} \leq \left\| \underbrace{S_\rho^{-1}(z_r, \mathbf{0}_{\mathcal{A}})}_{\in \mathcal{B}^c} + \underbrace{S_\rho^{-1}(\mathbf{0}_{n_x - \mathcal{A}}, z_q)}_{\in \mathcal{B}} \right\|_{\mathcal{B}} = \|S_\rho^{-1}(z_r, \mathbf{0}_{\mathcal{A}})\|_{\mathcal{B}} \leq \|S_\rho^{-1}(z_r, \mathbf{0}_{\mathcal{A}})\| \leq \|S_\rho^{-1}\| \|z_r\|. \quad (16)$$

Notice that z_r is the state of the reduced system associated with the nominal system (see [10, Section IV.B]). Since our choice of the nominal system output \tilde{y}_ρ , stated in (13), yields $\mathcal{B}_{\tilde{y}_\rho} = \mathbf{0}_{n_{\tilde{y}_\rho}}$, therefore the reduced system output equals \tilde{y}_ρ . Thus, the inputs (e, ω) and the output \tilde{y}_ρ of the reduced and nominal system are exactly the same. The reduced system is basically

$$\begin{aligned} \dot{z}_r &= A_\sigma^{\text{cl},r} z_r + B_\sigma^{\text{cl},r} e + B_\sigma^r \omega, \\ \tilde{y}_\rho &= \overline{C_\sigma^r z_r} + \omega. \end{aligned} \quad (17)$$

For explicit expressions of $A_\sigma^{\text{cl},r}$, $B_\sigma^{\text{cl},r}$, B_σ^r and C_σ^r see [10, Section IV.B]. In other words, the reduced system is merely a different state-space realization (though a lower-dimensional realization) of the

input-output mapping of the nominal system. In addition, notice that (8) is in fact

$$\dot{e} = -C^{\text{cl}} \left(A_{\sigma}^{\text{cl}} S_{\sigma}^{-1}(z_r, z_q) + B_{\sigma}^{\text{cl}} e + \omega \right) = -C^{\text{cl}} \left(A_{\sigma}^{\text{cl}} S_{\sigma}^{-1}(z_r, \mathbf{0}_{\mathcal{A}}) + B_{\sigma}^{\text{cl}} e + \omega \right).$$

Since the results invoked below are stated in terms of the Euclidean norm, the reduced system allows us to utilize those results at once (i.e., we use $\|z_r\|$ rather than $\|x\|_{\mathcal{B}}$ and relate those two norms via (16)).

Theorem 3. *Suppose that the conditions of Theorem 2 hold and $\omega \equiv \mathbf{0}_{n_{\omega}}$. In addition, assume that L_{ρ} , $\rho \in \mathcal{P}$, is fixed. Then, the interconnection (17)-(8) is UGES. Consequently, the closed-loop system (7)-(8) is UGES w.r.t. $(\mathcal{B}, \mathbf{0}_{n_e})$.*

Proof. Provided in Appendix 6.6. □

To shorten the notation, we introduce $\chi := (z_r, e)$. According to Theorem 3, each subsystem in \mathcal{P} is UGES (i.e., UGES w.r.t. $(\mathcal{B}, \mathbf{0}_{n_e})$ when considering x instead of z_r as the nominal system state). Let us now apply [19, Theorem 15.3.] to each subsystem in \mathcal{P} . From (50) we infer that the flow and jump maps are Lipschitz continuous and are zero at zero. In addition, jump times t_i 's are predefined (i.e., time-triggered according to Protocol 1 and do not depend on the actual solution of the system as long as the topology is fixed), and such that $0 < t_1 < t_2 < \dots < t_i$ and $\lim_{i \rightarrow \infty} t_i = \infty$ hold. Consequently, all conditions of [19, Theorem 15.3.] are met. From [19, Theorem 15.3.], we know that there exist functions $V_{\rho} : \mathbb{R} \times \mathbb{R}^{n_{z_r} + n_e} \rightarrow \mathbb{R}$, $\rho \in \mathcal{P}$, that are right-continuous in t and Lipschitz continuous in χ , and satisfy the following inequalities

$$c_{1,\rho} \|\chi\|^2 \leq V_{\rho}(t, \chi) \leq c_{2,\rho} \|\chi\|^2, \quad t \geq t_0, \quad (18)$$

$$D_{\rho}^{+} V_{\rho}(t, \chi) \leq -c_{3,\rho} \|\chi\|^2, \quad t \notin \mathcal{T}, \quad (19)$$

$$V_{\rho}(t^{+}, \chi^{+}) \leq V_{\rho}(t, \chi), \quad t \in \mathcal{T}, \quad (20)$$

for all $\chi \in \mathbb{R}^{n_{z_r} + n_e}$, where $c_{1,\rho}$, $c_{2,\rho}$ and $c_{3,\rho}$ are positive constants. These constants are readily obtained once k and l from Definition 1 are known (see the proof of [19, Theorem 15.3.]). In the above inequalities, $D_{\rho}^{+} V_{\rho}(t, \chi)$ denotes the upper right derivative of function V_{ρ} with respect to the solutions of the ρ^{th} system. The upper right derivative of V_{ρ} is given by

$$D_{\rho}^{+} V_{\rho}(t, \chi) := \limsup_{h \rightarrow 0, h > 0} \left(\frac{1}{h} [V_{\rho}(t + h, \chi(t + h)) - V_{\rho}(t, \chi(t))] \right),$$

where $\chi(t)$, $t \geq t_0$, denotes the trajectory of the ρ^{th} system. We now rewrite (18) and (19) as follows

$$c_1 \|\chi\|^2 \leq V_\rho(t, \chi) \leq c_2 \|\chi\|^2, \quad t \geq t_0, \quad (21)$$

$$D_\rho^+ V_\rho(t, \chi) \leq -2\lambda_0 V_\rho(t, \chi), \quad t \notin \mathcal{T}, \quad (22)$$

$$V_\rho(t, \chi) \leq \mu V_\varrho(t, \chi), \quad t \geq t_0, \quad (23)$$

for all $\chi \in \mathbb{R}^{n_{z_r} + n_e}$ and all $\rho, \varrho \in \mathcal{P}$, where

$$c_1 = \min_{\rho \in \mathcal{P}} c_{1,\rho} > 0, \quad c_2 = \max_{\rho \in \mathcal{P}} c_{2,\rho} > 0, \quad \lambda_0 = \min_{\rho \in \mathcal{P}} \frac{c_{3,\rho}}{2c_{1,\rho}} > 0, \quad \mu = \max_{\rho, \varrho \in \mathcal{P}} \frac{c_{2,\rho}}{c_{1,\varrho}} > 0.$$

Notice that $\mu > 1$ in the view of interchangeability of ρ and ϱ in (23). Following ideas from [23] and [24], we obtain the following result:

Theorem 4. *Consider the family of m systems for which (20), (21), (22) and (23) hold. Then the resulting switched system is UGES for every switching signal σ with average dwell-time*

$$\tau_a > \frac{\ln \mu}{2\lambda_0} \quad (24)$$

and N_0 arbitrary.

Proof. See Appendix 6.7. □

Corollary 1. *The MAN objective in the sense of Definition 5 is UGES w.r.t. $(\mathcal{B}, \mathbf{0}_{n_e})$ for every switching signal σ with the average dwell-time (24) and N_0 arbitrary.*

Proof. This proof is akin to the last part of the proof for Theorem 3. □

4.2.2 Switching with Disturbances

Let us now examine the MAN properties when $\omega \neq \mathbf{0}_{n_\omega}$. Notice that impulsive switched systems can be interpreted as time-varying impulsive systems. From Theorem 4 we infer that the corresponding state transition matrix $\Phi(t, t_0)$ satisfies

$$\|\Phi(t, t_0)\| \leq k \exp(-l(t - t_0)), \quad (25)$$

where $k = \sqrt{\frac{c_2}{c_1} \mu^{N_0}}$ and $l = \lambda$ for some $\lambda \in (0, \lambda_0)$. For the explicit form of state transition matrices of linear time-varying impulsive systems refer to [19, Chapter 3]. From the corresponding variation of

constants formula (see [19, Chapter 3])

$$\chi(t) = \Phi(t, t_0)\chi(0) + \int_{t_0}^t \Phi(t, s)[B_\sigma^{\text{r}\top} - C^{\text{cl}\top}]^\top \omega(s) ds,$$

and (25), we obtain

$$\|\chi(t)\| \leq k \exp(-l(t - t_0))\|\chi(0)\| + bk \int_{t_0}^t \exp(-l(t - s))\|\omega(s)\| ds,$$

where $\max_{\rho \in \mathcal{P}} \| [B_\rho^{\text{r}\top} - C^{\text{cl}\top}] \| \leq b$. Since $t \geq t_0$, therefore $\int_{t_0}^t \exp(-l(t - s)) ds \leq 1/l$ for any t_0 . Using [30, Theorem 12.2], we infer that the switched system of interest is *uniformly bounded-input bounded-state* stable which in turn implies ISS (refer to [3, Theorem 2.35 & Remark 2.36] for more details). Likewise, \mathcal{L}_p -stability from ω to (z_r, e) is obtained following the lines of [31]. We conclude the above discussion in the following theorem.

Theorem 5. *The MAN objective in the sense of Definition 5 is ISS and \mathcal{L}_p -stable w.r.t. $(\mathcal{B}, \mathbf{0}_{n_e})$ from ω to (x, e) for every switching signal σ with the average dwell-time (24) and N_0 arbitrary.*

Remark 5. *Recall that changes of the topology in $[t_i, t_{i+1})$, where $t_i, t_{i+1} \in \mathcal{T}$, remain unnoticed until t_{i+1} (or even later). Therefore, if $\min_{\rho \in \mathcal{P}} \tau_\rho \geq \tau_a$, then we effectively have that the switched system of interest is UGES for any switching signal. Obviously, we want to obtain τ_ρ 's as large as possible. This is yet another motivation for developing self-triggered control policies.*

Remark 6. *The above result is similar to the well-known result of [32]. The difference is that [32] considers continuous communication among agents. In fact, the main result of [32] is a special case of ours when $\tau_\rho \rightarrow 0$ for all $\rho \in \mathcal{P}$. Therefore, Theorem 5 generalizes the main result of [32] towards more realistic networking artifacts.*

5 Case Study: Single-Integrator Consensus

In this section we employ the results of Section 4 to examine performance vs. lifetime trade-offs for the single-integrator consensus problem (refer to [10] and the references therein). Afterwards, our theoretical predictions are experimentally verified using a set of wireless sensor platforms. We point out that other theoretical trade-offs (e.g., those involving T_ρ and $\|L_\rho\|$), performance metrics (e.g., time-efficiency and energy-efficiency as in [33]) or MAN tasks can be analyzed along the same lines. Alas, specifics of each of these analyses hinder unifying trade-off results in the spirit of Section 4. Accordingly, this section focuses on a subset of the cooperative tasks from Section 4.

As demonstrated in [10], the single-integrator consensus problem leads to $A_\sigma^{\text{cl}} = B_\sigma^{\text{cl}} = -k(L_\sigma \otimes \mathbf{I}_{n_\xi})$ and $C^{\text{cl}} = \mathbf{I}_{n_x}$, where k is a positive control gain and \otimes denotes the Kronecker product. Among several other topologies that satisfy Assumption 2, we work out the methodology from Section 4 on L_ρ , given by (9), and

$$L_\varrho = \begin{bmatrix} 1 & -1 & 0 & 0 & 0 \\ 0 & 1 & -1 & 0 & 0 \\ 0 & 0 & 1 & 0 & -1 \\ -1 & 0 & 0 & 1 & 0 \\ 0 & 0 & -1 & -1 & 2 \end{bmatrix}.$$

Algorithm 1 yields $\mathcal{P}_\varrho^1 = \{1, 3\}$, $\mathcal{P}_\varrho^2 = \{2, 4\}$ and $\mathcal{P}_\varrho^3 = \{5\}$. When $n_\xi = 1$, the corresponding substitution matrices are

$$S_\rho = \begin{bmatrix} 0.0166 & -0.3979 & 0.06 & 0.1306 & 0.1906 \\ 0.1558 & 0.1322 & -0.2684 & 0.1243 & -0.1440 \\ -1.4166 & 0.1979 & -0.4600 & 1.0694 & 0.6094 \\ 1.3333 & 0 & 0 & -1.3333 & 0 \\ 0.0667 & 0.2 & 0.4 & 0.1333 & 0.2 \end{bmatrix},$$

$$S_\varrho = \begin{bmatrix} -0.1994 & -0.3032 & 0.1994 & 0.1141 & 0.1891 \\ 0.2025 & -0.1625 & -0.2025 & 0.2051 & -0.0426 \\ 0.5327 & -0.3635 & -0.5327 & -0.7807 & 1.1442 \\ -0.5 & 0.5 & 0 & 0.5 & -0.5 \\ 0.1667 & 0.1667 & 0.3333 & 0.1667 & 0.1667 \end{bmatrix},$$

yielding the reduced closed-loop matrices in (17)

$$A_\rho^{\text{cl,r}} = k \begin{bmatrix} -1.1226 & 0.7449 & 0 & 0 \\ -0.7449 & -1.1226 & 0 & 0 \\ 0 & 0 & -2.7549 & 0 \\ 0 & 0 & 0 & -3 \end{bmatrix}, \quad A_\varrho^{\text{cl,r}} = k \begin{bmatrix} -0.7672 & 0.7926 & 0 & 0 \\ -0.7926 & -0.7672 & 0 & 0 \\ 0 & 0 & -2.4656 & 0 \\ 0 & 0 & 0 & -2 \end{bmatrix},$$

$$B_\rho^{\text{cl,r}} = k \begin{bmatrix} 0.0974 & 0.5451 & -0.2672 & -0.0540 & -0.3213 \\ -0.1873 & 0.1479 & 0.2566 & -0.2369 & 0.0197 \\ 3.9026 & -0.5451 & 1.2672 & -2.9460 & -1.6787 \\ -4 & 0 & 0 & 4 & 0 \end{bmatrix},$$

$$B_\varrho^{\text{cl,r}} = k \begin{bmatrix} 0.3134 & 0.1038 & -0.3134 & 0.0751 & -0.1789 \\ 0.0027 & 0.3650 & -0.0027 & -0.2478 & -0.1172 \\ -1.3134 & 0.8962 & 1.3134 & 1.9249 & -2.8211 \\ 1 & -1 & 0 & -1 & 1 \end{bmatrix},$$

$$B_\rho^{\text{r}} = \begin{bmatrix} 0.0166 & -0.3979 & 0.0600 & 0.1306 & 0.1906 \\ 0.1558 & 0.1322 & -0.2684 & 0.1243 & -0.1440 \\ -1.4166 & 0.1979 & -0.4600 & 1.0694 & 0.6094 \\ 1.3333 & 0 & 0 & -1.3333 & 0 \end{bmatrix},$$

$$B_\varrho^{\text{r}} = \begin{bmatrix} -0.1994 & -0.3032 & 0.1994 & 0.1141 & 0.1891 \\ 0.2025 & -0.1625 & -0.2025 & 0.2051 & -0.0426 \\ 0.5327 & -0.3635 & -0.5327 & -0.7807 & 1.1442 \\ -0.5 & 0.5 & 0 & 0.5 & -0.5 \end{bmatrix},$$

$$C_\rho^{\text{r}} = k \begin{bmatrix} -2.7549 & -1.4897 & 0.5098 & -0.75 \\ 1.4473 & -1.8694 & -0.8946 & -0.75 \\ 1.2151 & 1.3071 & 1.5698 & 1.5 \\ -2.7549 & -1.4897 & 0.5098 & 1.5 \\ -1.1226 & 0.7449 & -2.7549 & -3 \end{bmatrix}, \quad C_\varrho^{\text{r}} = k \begin{bmatrix} 0.1084 & -1.9541 & 0.7832 & 2 \\ 1.5739 & -0.3690 & -1.1479 & -2 \\ 0.6588 & 1.1615 & 1.6823 & 2 \\ -2.2328 & -0.7926 & -0.5344 & -2 \\ -0.7672 & 0.7926 & -2.4656 & -2 \end{bmatrix}, \quad (26)$$

while the matrix in (12) becomes

$$A_\rho^* = \begin{bmatrix} 2 & 1 & 0 & 1 & 0 \\ 1 & 1 & 1 & 1 & 0 \\ 0 & 1 & 1 & 0 & 1 \\ 1 & 1 & 0 & 2 & 1 \\ 0 & 0 & 1 & 1 & 2 \end{bmatrix}, \quad A_\varrho^* = \begin{bmatrix} 1 & 1 & 0 & 1 & 0 \\ 1 & 1 & 1 & 0 & 0 \\ 0 & 1 & 1 & 0 & 1 \\ 1 & 0 & 0 & 1 & 1 \\ 0 & 0 & 1 & 1 & 2 \end{bmatrix}.$$

5.1 Performance vs. Lifetime Trade-Offs

For a fixed topology, i.e., $\sigma(t) \equiv \rho$, a stabilizing τ_ρ yields (49). Notice that \tilde{K} and $\tilde{\gamma}$ in (49) are functions of both τ_ρ and the control gain k . In the interest of brevity, suppose that $p \in [1, \infty)$ and $A_\rho^{\text{cl,r}}$ is a normal matrix for each $\rho \in \mathcal{P}$. For instance, the latter is fulfilled whenever the algebraic and geometric multiplicity of each eigenvalue of A_ρ^{cl} coincide (which is the case for L_ρ and L_ϱ considered

above). Considering τ_ρ and k as variables, let us now determine dominant growth rates for K_ρ , γ_ρ , K_ρ^e , γ_ρ^e , K_ρ^d and γ_ρ^d that constitute \tilde{K} and $\tilde{\gamma}$ in (49).

From [20, Corollary 5.2.], (26), (14) and (15) we obtain

$$\begin{aligned} O(K_\rho) &= kO(K_\rho^d) = kO\left(\left(\lambda_{\max}(P_\rho)\right)^{\frac{1}{p}} \sqrt{\frac{\lambda_{\max}(P_\rho)}{\lambda_{\min}(P_\rho)}}\right), & O(\gamma_\rho) &= kO(\gamma_\rho^d) = kO\left(k \frac{\lambda_{\max}^2(P_\rho)}{\lambda_{\min}(P_\rho)}\right), \\ O(K_\rho^e) &= \frac{\exp(k\tau_\rho)}{k(2 - \exp(k\tau_\rho))}, & O(\gamma_\rho^e) &= \frac{\exp(2k\tau_\rho)}{k(2 - \exp(k\tau_\rho))}, \end{aligned}$$

where P_ρ is the solution of the Lyapunov equation $P_\rho A_\rho^{\text{cl,r}} + (A_\rho^{\text{cl,r}})^\top P_\rho = -\mathbf{I}_{n_x}$. Let us introduce $A_\rho^s := A_\rho^{\text{cl,r}} + (A_\rho^{\text{cl,r}})^\top$. Employing [34, (70) & (88)], we obtain $\lambda_{\min}(P_\rho) \geq \frac{1}{2\|A_\rho^{\text{cl,r}}\|}$ and $\lambda_{\max}(P_\rho) \leq \frac{-2}{\lambda_{\max}(A_\rho^s)}$. According to [35, Problem VII.6.4.], we know that $\lambda_{\max}(A_\rho^s) < 0$ since $A_\rho^{\text{cl,r}}$ is Hurwitz by construction. Moreover, $-\lambda_{\max}(A_\rho^s)$ equals the smallest singular value, denoted σ_{\min} , of A_ρ^s . The work in [36] provides $\sigma_{\min}(A_\rho^s) \geq \frac{|\det(A_\rho^s)|}{\sqrt{\text{trace}(A_\rho^{s\top} A_\rho^s)}}$. Using

$$\sqrt{\text{trace}(A_\rho^{s\top} A_\rho^s)} = \sqrt{\sum_{i=1}^{n_z} (\sigma_i(A_s))^2} \leq \sum_{i=1}^{n_z} \sigma_i(A_s) \leq n_{z_r} \|A_\rho^s\| \leq 2n_{z_r} \|A_\rho^{\text{cl,r}}\|$$

and the Marcus-de Oliviera conjecture from [35, p.184], we infer that the lower bound of $\sigma_{\min}(A_\rho^s)$ is a polynomial in k of order n_{z_r} . Thus, $O(K_\rho)$, $O(\gamma_\rho)$, $O(K_\rho^d)$ and $O(\gamma_\rho^d)$ are polynomials in k . Since $O(K_\rho^e)$ and $O(\gamma_\rho^e)$ contain exponential terms, their impact on the growth rates of \tilde{K} and $\tilde{\gamma}$ is predominant. Now, it is straightforward to show that the dominant growth rates of \tilde{K} and $\tilde{\gamma}$ are given by

$$O(\tilde{K}) = O(\tilde{\gamma}) = \frac{1}{k^\alpha (\varkappa - \exp(k\tau_\rho))}, \quad (27)$$

where $\alpha > 0$ while \varkappa is a positive constant whose actual value is irrelevant for our purposes herein. However, we point out that \varkappa is a function of L_ρ , agent dynamics and the selected decentralized control law. In order for (27) to be finite, the following needs to hold

$$\tau_\rho \in \left(0, \frac{\ln \varkappa}{k}\right), \quad (28)$$

which is in line with Theorem 1. Let us measure the MAN performance in terms of the time to reach (i.e., convergence rate) the MAN objective starting from some $(x(t_0), e(t_0))$ and in the presence of disturbance ω (refer to (49)).

From [13] and [10] we know there is an element of the set $\left(0, \frac{\ln \varkappa}{k}\right)$, denoted τ_ρ^{\max} , such that any

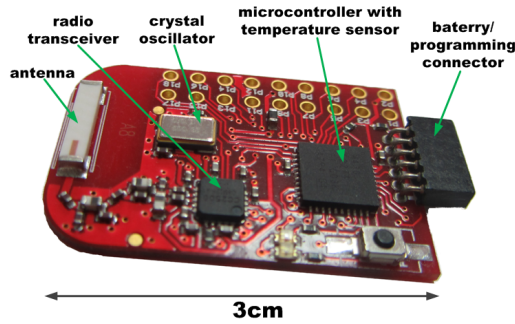


Figure 6: eZ430-RF2500 WSN node used in the experimental setup.

$\tau_\rho < \tau_\rho^{\max}$ stabilizes the control system of interest. Apparently, an increase in the control gain k decreases τ_ρ^{\max} . From (49) and (27) one concludes that, for a fixed k , the greater τ_ρ (i.e., greater \tilde{K} and $\tilde{\gamma}$) becomes, the smaller the rate of convergence towards the MAN objective becomes and the closed-loop system becomes more susceptible to disturbances/noise. On the other hand, the rate of convergence and disturbance sensitivity might be decreased by increasing k which in turn requires a smaller τ_ρ (i.e., more frequent information exchange). Nevertheless, a decrease in k might impair the MAN performance and disturbance rejection due to k^α in (27). Therefore, one needs to carefully balance between performance and energy needs. It might even turn out that the hardware at hand cannot deliver information at a rate below τ_ρ^{\max} . In that case, one should decrease k or augment \varkappa by changing the underlying communication topology, control law or system dynamics. Alternatively, one could seek for more advanced hardware. Lastly, in light of Theorem 5, the same inference about performance vs. resource consumption holds for time-varying topologies with switching signals satisfying the associated average dwell-time condition.

5.2 Experimental Setup

We select eZ430-RF2500 wireless sensor nodes because they offer a fairly short time window of activity for transmitting/receiving a message. In addition, these nodes are quite affordable and have modest energy requirements [37]. On the other hand, due to simplicity of the WSN nodes, the topology discovery algorithm [27] is not yet implemented and time-varying topologies are not examined experimentally. For numerical simulations involving switching topologies, albeit without agent partitions, refer to [10].

Each eZ430-RF2500 node (Figure 6) is a very low-power wireless platform built around an MSP430 microcontroller and CC2500 transceiver [38]. The ultra low-power MSP430 is a 16-bit microcontroller with 5 low-power operating modes. It is equipped with a digitally controlled oscillator (DCO) as well as with an internal very-low-power low-frequency oscillator (VLO) used in low-power operating modes. Besides the internal clock source, MSP430 also supports external crystal oscillators. Information

about power consumption and oscillator characteristics are shown in Table 1. More information about typical drifts for commercial clock sources and procedures regarding how to suppress them can be found in [26].

The CC2500 is a 2.4-GHz RF transceiver implementing SimpliciTI communication protocol with 250 kbps data rate. This proprietary stack of Texas Instruments is much simpler than the generally used IEEE 802.15.4/ZigBee protocol, requires less memory capacity and enables lower power consumption when the node is in the idle mode. It also has a much lower overhead in terms of additional headers per packet (only 14 extra bytes).

5.3 Energy Consumption

To characterize the energy consumption of the eZ430-RF2500, the node was connected to a laboratory power source providing 3 V, and a 10 Ω resistor was connected in series to the node. The current in the circuit was measured by a multimeter (Fluke 45), while the voltage drop on the resistor was captured with a digital oscilloscope (Rigol DS1102E). Node current consumption in different operating modes is shown in Table 2. Figure 7 shows the voltage drop (proportional to the node current consumption) on the resistor, presenting a sequence in which the node is receiving and then transmitting a packet. As pointed out in the figure, the time interval required to merely receive or transmit is about 780 μ s, but a significant amount of time is taken by switching between operating modes. The intrinsic platform-dependent functions (e.g., calibration, scanning the channel before sending, etc.) create an overhead. Due to this overhead, it takes 2.2 ms to broadcast or receive a message. This represents the hardware-dependent lower bound on τ_p .

The energy consumption of the node, denoted E_{node} , is the sum of the energy utilized in all operating modes and energy utilized for all transitions between operating modes, i.e.,

$$E_{\text{node}} = \sum_{\text{mode}} P_{\text{mode}} \cdot t_{\text{mode}} + \sum_{\text{trans}} P_{\text{trans}} \cdot t_{\text{trans}}, \quad (29)$$

Table 1: Current consumption and oscillator characteristics of MSP430 microcontroller.

Current consumption	active mode (at 1 MHz and 3.3 V)	about 300 μ A
	deepest low-power mode	about 500 nA
Oscillators	digitally controlled oscillator	+/-2% typical tolerance +/-5% maximal tolerance
	very-low-power low-frequency oscillator	frequency drift 0.5%/°C and 4%/V

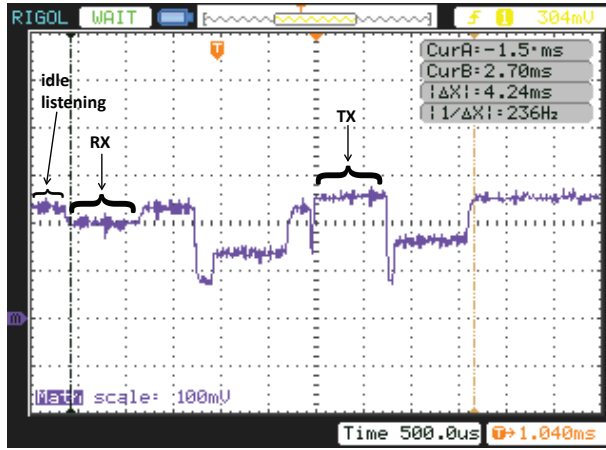


Figure 7: A sequence showing a node listening to the communication medium, then receiving a message and immediately transmitting another message afterwards. The packet has 2 B payload (total 24 B on the physical layer due to the stack and radio overhead). Transitions between operating modes present a significant overhead in time and energy. Notice that the power consumption of the radio when merely listening is almost the same (and even slightly higher!) as when actually receiving a packet. This finding also advocates the TDMA scheduling employing agent partitions.

where P_{mode} and t_{mode} represent power consumption of the node in a particular operation mode and the time spent in that mode, respectively. Taking into account the power consumption of a node from Table 2 and measuring the time intervals when staying in different modes and transitions (as in Figure 7), we estimate the long-term energy consumption of the node. In our experiment, each node was connected to a small-size battery providing 3 V and 1000 mAh. In the idle mode the radio was inactive while the microcontroller was active.

5.4 Experimental Results

We select $k = 1$, $p = 2$, randomly pick initial states that are further apart (see Figure 8(c)) and use these initial states in all experiments for a fair comparison. The single-integrator problem was implemented for various broadcasting intervals τ_ρ ranging from the lower physical limit of 2.2 ms to the experimental upper limit on the stabilizing intervals of 0.3 s. We point out that the theoretical upper bound on the stabilizing intervals τ_ρ , obtained via Section 4, is 0.033 s. Hence, the theoretically predicted τ_ρ^{max} is about 9 times more conservative than the experimental one.

Table 2: Current consumption of the eZ430-RF2500 node in different operating modes with a 3 V supply.

Component		Current consumption [mA]
microcontroller	transceiver	
on	on, RX	21.30
on	on, TX	25.11
on	off	3.00
off	off	0.001

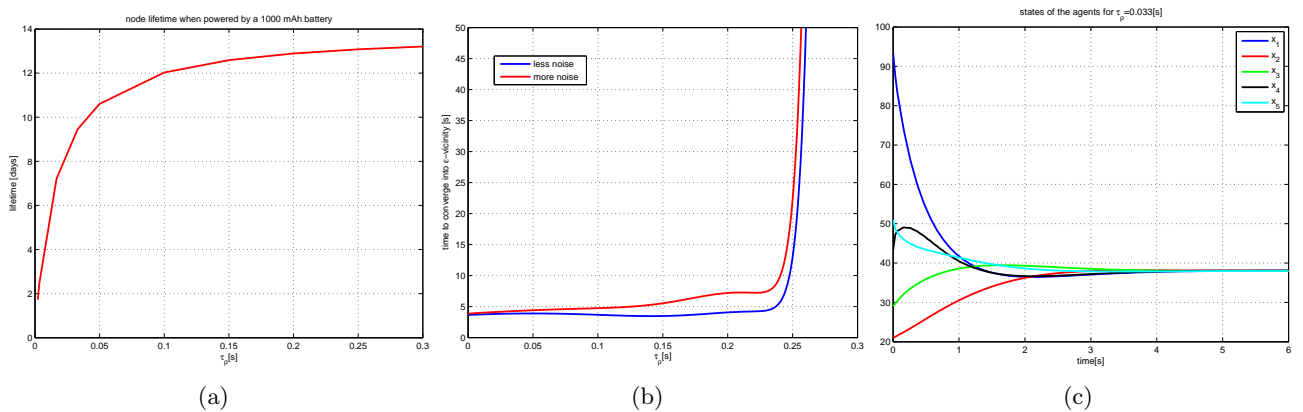


Figure 8: Experimental results that verify the theoretical exposition of Section 4: (a) Expected lifetime of the battery; (b) Time to converge into ϵ -vicinity of the consensus for $\epsilon = 0.4$; and, (c) States of the agents for $\tau_p = 0.033$ s.

As shown in Figure 4, each node cycles between the following modes: TX-idle-RX-idle-RX-idle-TX-..., and so on. Clearly, each cycle lasts for $T_\rho\tau_p$ seconds. The expected node lifetime, when powered by a 1000 mAh capacity battery, is shown in Figure 8(a) for different τ_p . The smaller the τ_p is, the greater the average power consumed in one cycle becomes. If we want to increase the lifetime of our device by increasing τ_p , the closed-loop system takes longer to reach ϵ -vicinity of consensus (see Figure 8(b)). In addition, a greater τ_p causes greater sensitivity to noise as shown in Figure 8(b). The smaller noise/disturbance level is hardware-dependent and arises from rounding the exchanged data to two decimal places. The greater noise/disturbance level is emulated by adding random numbers to the exchanged data. Those random numbers are drawn from the uniform distribution over the interval $[-1, 1]$. Since the nodes in our experiments are within 10 m from each other, hardware-specific sporadic losses of messages are negligible [39]. Nevertheless, an increase in lost messages can easily be compensated for according to Remark 4.

As predicted by (27), the graphs in Figures 8(a) and 8(b) are rather nonlinear with vertical and horizontal asymptotes; hence, considerable decreases of intertransmission intervals may not significantly improve performance while the corresponding expected lifetimes may be significantly shortened (and vice versa). The rationale behind this observation is that, as τ_p decreases, practically the same information are being exchanged in several consecutive intervals. Basically, upcoming (but costly) transmissions do not bring significantly different information; hence, the “old” information (preserved via the zero-order-hold strategy) are an adequate replacement for the “new” information.

Figure 8(c) brings experimentally obtained states of the agents for the theoretical $\tau_p^{\max} = 0.033$ s. Apparently, from Figures 8(a) and 8(b), we infer that the theoretical $\tau_p^{\max} = 0.033$ s provides an acceptable compromise between the time to converge and node lifetime.

6 Conclusion

In this paper, we devise a comprehensive self-triggered communication scheme for managing resources of MANs without compromising the original initial-condition-(in)dependent goal of the MANs. By extending the intervals of idleness of each agent, our communication scheme poses lesser demands on the agent resources (e.g., lowers the operating frequency and energy consumption). In addition, these resources can now be exploited for other activities (e.g., inter-network collaboration). However, extended intervals of idleness lead to degraded performance which manifests in decreased disturbance/noise resilience and increased convergence times. On the other hand, shorter intertransmission intervals may significantly decrease network lifetime while performance may not improve considerably. In addition, our experimental findings are in good accordance with the theoretical analyses and suggest that our theoretical bounds are not overly conservative and provide a reasonable performance vs. energy trade-off.

In the future, in light of [17], we plan to pose the performance vs. resource consumption trade-offs as an optimal control problem and solve it in a decentralized fashion. Likewise, due to [28], consideration of nonlinear agents is in order. Regarding the practical side of this work, the experiments indicate that it is important to keep agents' internal clocks synchronized. Evidently, the proposed scheme is suitable for clock synchronization during experiments; hence, it will be employed in the future. Finally, similar experiments will be carried out on our mobile robotics testbed.

Acknowledgment

This work has been supported by the European Community Seventh Framework Programme under grant No. 285939 (ACROSS). D. Tolić is partially supported by the Air Force Research Laboratory under agreement number FA8655-13-1-3055. The U.S. Government is authorized to reproduce and distribute reprints for Governmental purposes notwithstanding any copyright notation thereon.

The views and conclusions contained herein are those of the authors and should not be interpreted as necessarily representing the official policies or endorsements, either expressed or implied, of the Air Force Research Laboratory or the U.S. Government.

Appendix

6.1 Graph Theory

A *directed graph*, or digraph, is a pair $\mathcal{G} = (\mathcal{V}, \mathcal{E})$, where $\mathcal{V} = \{1, \dots, N\}$ is a nonempty set of *nodes* (or vertices) and $\mathcal{E} \subset \mathcal{V} \times \mathcal{V}$ is the set of the corresponding *edges*. When the edge (i, j) belongs to \mathcal{E} , it means that there is an information flow from the node i to the node j . We do not allow *self-loops*, i.e., edges that connect a vertex to itself. When both (i, j) and (j, i) belong to \mathcal{E} , we say that the *link* between i and j is *bidirectional*. Otherwise, the link between i and j is *unidirectional*. The set of *neighbors* of the node i is $\mathcal{N}_i = \{j \in \mathcal{V} : (j, i) \in \mathcal{E}\}$, which is all nodes that the node i can obtain information from. A *path* in a graph is a sequence of vertices such that from each of its vertices there is an edge to the next vertex in the sequence. A *cycle* in \mathcal{G} is a directed path with distinct nodes except for the starting and ending node. An *inclusive cycle* for an edge is a cycle that contains the edge on its path. A *directed tree* is a directed graph in which every node has exactly one parent except for one node. A *subgraph* $\mathcal{G}^s = (\mathcal{V}^s, \mathcal{E}^s)$ of \mathcal{G} is a graph such that $\mathcal{V}^s \subseteq \mathcal{V}$ and $\mathcal{E}^s \subseteq \mathcal{E} \cap (\mathcal{V}^s \times \mathcal{V}^s)$. A *directed spanning tree* \mathcal{G}^s of \mathcal{G} is a subgraph of \mathcal{G} such that \mathcal{G}^s is a directed tree and $\mathcal{V}^s = \mathcal{V}$. A graph \mathcal{G} *contains* a directed spanning tree if a directed spanning tree is a subgraph of \mathcal{G} .

Given a graph \mathcal{G} , the graph Laplacian matrix $L \in \mathbb{R}^{|\mathcal{V}| \times |\mathcal{V}|}$ is defined as

$$L = [l_{ij}], \quad l_{ij} = \begin{cases} -1, & j \in \mathcal{N}_i \\ |\mathcal{N}_i|, & j = i \\ 0, & \text{otherwise} \end{cases}.$$

6.2 From Agent Dynamics to Closed-Loop Dynamics

Consider N heterogeneous linear systems, i.e., agents, given by

$$\begin{aligned} \dot{\xi}_i &= A_i \xi_i + B_i u_i + \omega_i, \\ \zeta_i &= C_i \xi_i, \end{aligned} \tag{30}$$

where $\xi_i \in \mathbb{R}^{n_{\xi_i}}$ is the state, $u_i \in \mathbb{R}^{n_{\zeta}}$ is the input, $\zeta_i \in \mathbb{R}^{n_{\zeta}}$ is the output of the i^{th} system, $i \in \{1, 2, \dots, N\}$, and $\omega_i \in \mathbb{R}^{n_{\zeta}}$ reflects exogenous disturbances or unmodeled dynamics. In addition, A_i , B_i and C_i are matrices of appropriate dimensions. Since these agents are vertices of a communication graph, the set of all agents is denoted \mathcal{V} . Hence, $|\mathcal{V}| = N$. A common decentralized control policy is

given by

$$u_i = -K_i \sum_{j \in \mathcal{N}_i} [(\zeta_i - \zeta_j) - (d_i - d_j)], \quad (31)$$

where K_i is a $n_{u_i} \times n_\zeta$ matrix, \mathcal{N}_i denotes the set of neighbors of the i^{th} agent and $d_i \in \mathbb{R}^{n_\zeta}$ is the bias term. Next, let us define the following stack vectors $\xi := (\xi_1, \xi_2, \dots, \xi_N)$, $y := (\zeta_1, \zeta_2, \dots, \zeta_N)$, $d := (d_1, d_2, \dots, d_N)$ and $\omega := (\omega_1, \omega_2, \dots, \omega_N)$. Knowing the Laplacian matrix L_ρ of a communication graph \mathcal{G} , the closed-loop dynamic equation of (30) given the control law (31) becomes

$$\begin{aligned} \dot{\xi} &= A_\rho^{\text{cl}} \xi - B_\rho^{\text{cl}} d + \omega, \\ \zeta &= C^{\text{cl}} \xi, \end{aligned} \quad (32)$$

where $\rho \in \mathcal{P}$ denotes the subsystem associated with L_ρ , and

$$\begin{aligned} A_\rho^{\text{cl}} &= [A_{\rho,ij}^{\text{cl}}], \quad A_{\rho,ij}^{\text{cl}} = \begin{cases} A_i - l_{\rho,ii} B_i K_i C_i, & i = j \\ -l_{\rho,ij} B_i K_i C_j, & \text{otherwise} \end{cases}, \\ B_\rho^{\text{cl}} &= [B_{\rho,ij}^{\text{cl}}], \quad B_{\rho,ij}^{\text{cl}} = -l_{\rho,ij} B_i K_i, \\ C^{\text{cl}} &= \text{diag}(C_1, C_2, \dots, C_N), \end{aligned} \quad (33)$$

where $A_{\rho,ij}^{\text{cl}}$ and $B_{\rho,ij}^{\text{cl}}$ are matrix blocks whilst $\text{diag}(\cdot, \cdot, \dots, \cdot)$ indicates a diagonal matrix.

Remark 7. Using the Geršgorin circle theorem, the work in [40] provides sufficient conditions for A_ρ^{cl} to be Hurwitz. Applying these sufficient conditions to A_ρ^{cl} herein, we obtain that when

(i) $A_i - l_{\rho,ii} B_i K_i C_i$ is Hurwitz for all $i \in \{1, 2, \dots, N\}$, and

(ii) $\min_{\lambda_i \in \lambda(A_i - l_{\rho,ii} B_i K_i C_i)} |\lambda_i| \geq \sum_{j \in \mathcal{N}_i} \|B_i K_i C_j\|$,

where the set of all eigenvalues of a matrix is denoted $\lambda(\cdot)$, are fulfilled, the matrix A_ρ^{cl} is Hurwitz. Thus, by changing K_i 's for different topologies, one can ensure that A_ρ^{cl} remains Hurwitz.

When $\omega \equiv \mathbf{0}_{n_\omega}$, the equilibria of (32) satisfy

$$A_\rho^{\text{cl}} \xi = B_\rho^{\text{cl}} d. \quad (34)$$

It is well known that the above matrix equality is solvable if and only if $B_\rho^{\text{cl}} d$ is in the column space of A_ρ^{cl} . If this condition is not met, simply select different d_i 's. Notice that $d = \mathbf{0}_{n_d}$ or A_ρ^{cl} being Hurwitz immediately makes (34) solvable. Provided that (34) is solvable, we can find a particular solution ξ^{p}

to (34). The corresponding output is $\zeta^P = C^{\text{cl}}\xi^P$. Now, the substitutions $x = \xi - \xi^P$ and $y = \zeta - \zeta^P$ transform (32) into the equivalent system (6). Notice that one can change ζ^P by changing d . For example, one can change formations by changing d .

6.3 Introducing Intermittent Data Exchange

The control law (31) can be modified as follows:

$$u_i = -K_i \sum_{j \in \mathcal{N}_i} [(\hat{\zeta}_i - \hat{\zeta}_j) - (d_i - d_j)], \quad (35)$$

where signals $\hat{\zeta}_i : [t_0, \infty) \rightarrow \mathbb{R}^{n_x}$, $i \in \{1, \dots, N\}$, are piece-wise constant and right-continuous functions with jumps accompanying the data exchange instants and $t_0 \in \mathbb{R}$ is the initial time. In other words, the control signal u_i is driven by sampled zero-order-hold versions of the actual signals $\zeta_i : [t_0, \infty) \rightarrow \mathbb{R}^{n_x}$, $i \in \{1, \dots, N\}$. Now, let us introduce the error vector e as follows

$$e = \begin{bmatrix} e_1 \\ e_2 \\ \vdots \\ e_N \end{bmatrix} := \begin{bmatrix} \hat{\zeta}_1 - \zeta_1 \\ \hat{\zeta}_2 - \zeta_2 \\ \vdots \\ \hat{\zeta}_N - \zeta_N \end{bmatrix} = \hat{\zeta} - \zeta. \quad (36)$$

The above expression uses $\hat{\zeta} := (\hat{\zeta}_1, \hat{\zeta}_2, \dots, \hat{\zeta}_N)$. Taking e into account, the closed-loop dynamics (6) become (7). Since $\dot{\hat{\zeta}} = 0$ and $\dot{\zeta}^P = 0$, the corresponding error dynamics are (8).

6.4 Proof of Proposition 1

Proof. This proposition is proved by showing that

$$\| -C^{\text{cl}}(A_\rho^{\text{cl}}x + \omega) \|_{\mathcal{B}_{\hat{y}_\rho}} \geq \overline{\| -C^{\text{cl}}(A_\rho^{\text{cl}}x + \omega) \|_{\mathcal{B}_{\tilde{y}_\rho}}}, \quad (37)$$

where the sets $\mathcal{B}_{\hat{y}_\rho}$ and $\mathcal{B}_{\tilde{y}_\rho}$ are obtained via (3). Apparently, $\mathcal{B}_{\tilde{y}_\rho}$ may be constructed from $\mathcal{B}_{\hat{y}_\rho}$ by applying the $\bar{\cdot}$ operator to the elements of $\mathcal{B}_{\hat{y}_\rho}$. In addition, notice that $n_{\hat{y}_\rho} = n_{\tilde{y}_\rho}$. Now, the inequality (37) is obtained as follows. For each $i \in 1, \dots, n_{\tilde{y}}$, the reverse triangle inequality yields

$$\left| (-C^{\text{cl}}(A_\rho^{\text{cl}}x + \omega) - b_{\hat{y}_\rho})_i \right| \geq \left| |(-C^{\text{cl}}(A_\rho^{\text{cl}}x + \omega))_i| - |(b_{\hat{y}_\rho})_i| \right|,$$

where $b_{\tilde{y}_\rho} \in \mathcal{B}_{\tilde{y}_\rho}$ and $(\cdot)_i$ denotes the i^{th} component of a vector. Hence,

$$\| -C^{\text{cl}}(A_\rho^{\text{cl}}x + \omega) - b_{\tilde{y}_\rho} \| \geq \| \overline{-C^{\text{cl}}(A_\rho^{\text{cl}}x + \omega) - b_{\tilde{y}_\rho}} \|,$$

yielding

$$\inf_{b_{\tilde{y}_\rho} \in \mathcal{B}_{\tilde{y}_\rho}} \| -C^{\text{cl}}(A_\rho^{\text{cl}}x + \omega) - b_{\tilde{y}_\rho} \| \geq \inf_{b_{\tilde{y}_\rho} \in \mathcal{B}_{\tilde{y}_\rho}} \| \overline{-C^{\text{cl}}(A_\rho^{\text{cl}}x + \omega) - b_{\tilde{y}_\rho}} \| = \inf_{b_{\tilde{y}_\rho} \in \mathcal{B}_{\tilde{y}_\rho}} \| \overline{-C^{\text{cl}}(A_\rho^{\text{cl}}x + \omega) - b_{\tilde{y}_\rho}} \|,$$

which is equivalent to (37). \square

6.5 Proof of Theorem 2

Proof. According to [10, Section IV.D], the state x of system (7) is \mathcal{L}_p -detectable w.r.t. \mathcal{B} from input (ω, e) and from any output \dot{y}_ρ , i.e., there exist K_ρ^d and γ_ρ^d such that

$$\|x[t_0, t]\|_{p, \mathcal{B}} \leq K_\rho^d \|x(t_0)\|_{\mathcal{B}} + \gamma_\rho^d \|\dot{y}_\rho[t_0, t]\|_{p, \mathcal{B}_y} + \gamma_\rho^d \|\omega[t_0, t]\|_p, \quad (38)$$

for any $t \geq t_0$. In addition, from the assumptions of the theorem we have:

$$\|\tilde{y}_\rho[t_0, t]\|_{p, \mathcal{B}_{\tilde{y}_\rho}} \leq K_\rho \|x(t_0)\|_{\mathcal{B}} + \gamma_\rho \|(\omega, e)[t_0, t]\|_p, \quad (39)$$

$$\|e[t_0, t]\|_p \leq K_\rho^e \|e(t_0)\| + \gamma_\rho^e \|\tilde{y}_\rho[t_0, t]\|_p, \quad (40)$$

for all $t \geq t_0$. Notice that (39) involves $\|\tilde{y}_\rho[t_0, t]\|_{p, \mathcal{B}_{\tilde{y}_\rho}}$ while (40) involves $\|\tilde{y}_\rho[t_0, t]\|_p$. Therefore, in general, the small-gain theorem is not applicable to interconnections of systems that are \mathcal{L}_p -stable w.r.t. sets. However, our choice of the output \tilde{y}_ρ , stated in (13), yields $\mathcal{B}_{\tilde{y}_\rho} = \mathbf{0}_{n_{\tilde{y}_\rho}}$. In other words, $\|\tilde{y}_\rho[t_0, t]\|_p = \|\tilde{y}_\rho[t_0, t]\|_{p, \mathcal{B}_{\tilde{y}_\rho}}$. Next, notice that $\|(\omega, e)[t_0, t]\|_p \leq \|\omega[t_0, t]\|_p + \|e[t_0, t]\|_p$. We now apply the small-gain theorem to (39)-(40) obtaining

$$\|\tilde{y}_\rho[t_0, t]\|_p \leq \frac{1}{1 - \gamma_\rho \gamma_\rho^e} [K_\rho \|x(t_0)\|_{\mathcal{B}} + \gamma_\rho K_\rho^e \|e(t_0)\| + \gamma_\rho \|\omega[t_0, t]\|_p], \quad (41)$$

$$\|e[t_0, t]\|_p \leq \frac{1}{1 - \gamma_\rho \gamma_\rho^e} [\gamma_\rho^e K_\rho \|x(t_0)\|_{\mathcal{B}} + K_\rho^e \|e(t_0)\| + \gamma_\rho \gamma_\rho^e \|\omega[t_0, t]\|_p]. \quad (42)$$

Merging (38) and (41), we obtain:

$$\|x[t_0, t]\|_{p, \mathcal{B}} \leq \left(\frac{K_\rho \gamma_\rho^d}{1 - \gamma_\rho \gamma_\rho^e} + K_\rho^d \right) \|x(t_0)\|_{\mathcal{B}} + \frac{K_\rho^e \gamma_\rho \gamma_\rho^d}{1 - \gamma_\rho \gamma_\rho^e} \|e(t_0)\| + \left(\frac{\gamma_\rho \gamma_\rho^d}{1 - \gamma_\rho \gamma_\rho^e} + \gamma_\rho^d \right) \|\omega[t_0, t]\|_p. \quad (43)$$

Now, we use the following equality:

$$\|(x, e)[t_0, t]\|_{p,(\mathcal{B}, \mathbf{0}_{n_e})} = \|(x, \mathbf{0}_{n_e})[t_0, t] + (\mathbf{0}_{n_x}, e)[t_0, t]\|_{p,(\mathcal{B}, \mathbf{0}_{n_e})}. \quad (44)$$

It is easily shown (simply follow the proof for the classical Minkowski inequality [41, Chapter 6] and the fact that $\|\cdot\|_{\mathcal{B}}$ is a seminorm) that

$$\begin{aligned} \|(x, \mathbf{0}_{n_e})[t_0, t] + (\mathbf{0}_{n_x}, e)[t_0, t]\|_{p,(\mathcal{B}, \mathbf{0}_{n_e})} &\leq \|(x, \mathbf{0}_{n_e})[t_0, t]\|_{p,(\mathcal{B}, \mathbf{0}_{n_e})} + \|(\mathbf{0}_{n_x}, e)[t_0, t]\|_{p,(\mathcal{B}, \mathbf{0}_{n_e})} \\ &= \|x[t_0, t]\|_{p, \mathcal{B}} + \|e[t_0, t]\|_p \end{aligned} \quad (45)$$

holds. In fact, one can think of (45) as a variant of the classical Minkowski inequality. Combining (42), (43), (44) and (45) yields

$$\|(x, e)[t_0, t]\|_{p,(\mathcal{B}, \mathbf{0}_{n_e})} \leq K_1 \|x(t_0)\|_{\mathcal{B}} + K_2 \|e(t_0)\| + \tilde{\gamma} \|\omega[t_0, t]\|_p, \quad (46)$$

where $K_1 = \frac{\gamma_\rho^e K_\rho + \gamma_\rho^d K_\rho}{1 - \gamma_\rho \gamma_\rho^e} + K_\rho^d$, $K_2 = \frac{K_\rho^e + K_\rho^e \gamma_\rho \gamma_\rho^d}{1 - \gamma_\rho \gamma_\rho^e}$ and $\tilde{\gamma} = \frac{\gamma_\rho \gamma_\rho^e + \gamma_\rho \gamma_\rho^d}{1 - \gamma_\rho \gamma_\rho^e} + \gamma_\rho^d$. We proceed by obtaining the following expression:

$$\begin{aligned} \|x(t_0)\|_{\mathcal{B}} + \|e(t_0)\| &= \inf_{b \in \mathcal{B}} \|x(t_0) - b\| + \|e(t_0)\| \leq \inf_{b \in \mathcal{B}} \left(\sum_{i=1}^{n_x} |x_i(t_0) - b_i| \right) + \sum_{i=1}^{n_e} |e_i(t_0) - 0| \\ &= \inf_{b \in \mathcal{B}} \left(\sum_{i=1}^{n_x} |x_i(t_0) - b_i| + \sum_{i=1}^{n_e} |e_i(t_0) - 0| \right) \leq \sqrt{n_x + n_e} \inf_{b \in \mathcal{B}} \left(\|(x(t_0), e(t_0)) - (b, \mathbf{0}_{n_e})\| \right) \\ &= \sqrt{n_x + n_e} \|(x(t_0), e(t_0))\|_{(\mathcal{B}, \mathbf{0}_{n_e})}. \end{aligned} \quad (47)$$

In the above derivation, we use the following inequalities

$$\sqrt{\sum_{i=1}^{n_\vartheta} |\vartheta_i|^2} \leq \sum_{i=1}^{n_\vartheta} |\vartheta_i| \leq \sqrt{n_\vartheta} \sqrt{\sum_{i=1}^{n_\vartheta} |\vartheta_i|^2}, \quad (48)$$

where $\vartheta = (\vartheta_1, \dots, \vartheta_{n_\vartheta}) \in \mathbb{R}^{n_\vartheta}$. Finally, putting together (46) and (47), we obtain

$$\|(x, e)[t_0, t]\|_{p,(\mathcal{B}, \mathbf{0}_{n_e})} \leq \tilde{K} \|(x(t_0), e(t_0))\|_{(\mathcal{B}, \mathbf{0}_{n_e})} + \tilde{\gamma} \|\omega[t_0, t]\|_p, \quad (49)$$

where $\tilde{K} := \sqrt{n_x + n_e} \max\{K_1, K_2\}$. □

6.6 Proof of Theorem 3

Proof. Let us show that (17) and (8) satisfy the assumptions of [22, Theorem 2.5]. In other words, we show that there exist nonnegative constants L_1, L_2, L_3 and L_4 such that

$$\left. \begin{aligned} \|A_\rho^{\text{cl},r} z_r + B_\rho^{\text{cl},r} e\| &\leq L_1(\|z_r\| + \|e\|) \\ \|C^{\text{cl}} A_\rho^{\text{cl}} S_\rho^{-1}(z_r, z_q) + C^{\text{cl}} B_\rho^{\text{cl}} e\| &\leq L_2(\|z_r\| + \|e\|) \\ \|z_r^+(t)\| &\leq L_3 \|z_r(t)\| \\ \|e^+(t)\| &\leq L_4 \|e(t)\| \end{aligned} \right\} \quad (50)$$

for all $z_r \in \mathbb{R}^{n_x - \mathcal{A}}$, all $e \in \mathbb{R}^{n_e}$ and each $\rho \in \mathcal{P}$. Notice that z_r does not experience jumps when new information arrives; hence, one can take $L_3 = 1$. From (10) it follows that the last inequality is satisfied with $L_4 = 1$. It is straightforward to show that $L_1 = \max\{\|A_\rho^{\text{cl},r}\|, \|B_\rho^{\text{cl},r}\|\}$ and $L_2 = \max\{\|C^{\text{cl}} A_\rho^{\text{cl}} S_\rho^{-1}\|, \|C^{\text{cl}} B_\rho^{\text{cl}}\|\}$ satisfy the above inequalities. The UGES property of (z_r, e) follows from [22, Theorem 2.5], i.e., there exist $k, l > 0$ such that $\|(z_r, e)(t)\| \leq k \exp(-l(t - t_0)) \|(z_r, e)(t_0)\|$ for all $t \geq t_0$ and for any $(z_r, e)(t_0)$.

Lastly, for all $t \geq t_0$ and for any $(x, e)(t_0)$ we have

$$\begin{aligned} \|(x, e)(t)\|_{(\mathcal{B}, \mathbf{0}_{n_e})} &\stackrel{\text{seminorm}}{\leq} \|(x(t), \mathbf{0}_{n_e})\|_{(\mathcal{B}, \mathbf{0}_{n_e})} + \|(\mathbf{0}_{n_x}, e(t))\|_{(\mathcal{B}, \mathbf{0}_{n_e})} \leq \|x(t)\|_{\mathcal{B}} + \|e(t)\| \leq \\ &\stackrel{(16)}{\leq} \|S_\rho^{-1}\| \|z_r(t)\| + \|e(t)\| \leq \max\{\|S_\rho^{-1}\|, 1\} (\|z_r(t)\| + \|e(t)\|) \leq \\ &\stackrel{(48)}{\leq} \max\{\|S_\rho^{-1}\|, 1\} \sqrt{n_{z_r} + n_e} \|(z_r, e)(t)\| \\ &\leq k \max\{\|S_\rho^{-1}\|, 1\} \sqrt{n_{z_r} + n_e} \exp(-l(t - t_0)) \|(z_r, e)(t_0)\| \\ &\leq k \max\{\|S_\rho^{-1}\|, 1\} \sqrt{n_{z_r} + n_e} \exp(-l(t - t_0)) (\|z_r(t_0)\| + \|e(t_0)\|) \\ &\leq k \max\{\|S_\rho^{-1}\|, 1\} \sqrt{n_{z_r} + n_e} \exp(-l(t - t_0)) (\|S_\rho\| \|P\| \|x(t_0)\|_{\mathcal{B}} + \|e(t_0)\|) \\ &\stackrel{(47)}{\leq} k_1 \exp(-l(t - t_0)) \|(x, e)(t_0)\|_{(\mathcal{B}, \mathbf{0}_{n_e})}, \end{aligned}$$

where P is the oblique projector onto \mathcal{B}^c along \mathcal{B} (refer to [10, Section IV.C] for more) and $k_1 := k \sqrt{n_{z_r} + n_e} \sqrt{n_x + n_e} \max\{\|S_\rho^{-1}\|, 1\} \max\{\|S_\rho\| \|P\|, 1\}$. \square

6.7 Proof of Theorem 4

Proof. This proof follows the proof of [23, Theorem 3.2]. Pick an arbitrary $T > 0$, let $t_0 := 0$, and denote the switching times on the interval $(0, T)$ by $t_1, \dots, t_{N_\sigma(T,0)}$. Consider the function $W(t) :=$

$\exp(2\lambda_0 t)V_{\sigma(t)}(t, \chi(t))$. On each interval $[t_j, t_{j+1})$ we have

$$D_{\sigma(t_j)}^+ W = 2\lambda_0 W + \exp(2\lambda_0 t)D_{\sigma(t_j)}^+ V_{\sigma(t_j)}(t, \chi) \leq 0$$

due to (22). Due to (20), when state jumps occur we have $V_{\sigma(t_j)}(t^+, \chi^+) \leq V_{\sigma(t_j)}(t, \chi)$ no matter whether the jump times coincide with the switching times or not. Therefore, W is nonincreasing between two switching times. This together with (20) and (23) yields

$$\begin{aligned} W(t_{j+1}) &= \exp(2\lambda_0 t_{j+1})V_{\sigma(t_{j+1})}(t_{j+1}, \chi(t_{j+1})) \leq \mu \exp(2\lambda_0 t_{j+1})V_{\sigma(t_j)}(t_{j+1}, \chi(t_{j+1})) \leq \\ &\leq \mu \exp(2\lambda_0 t_{j+1}^-)V_{\sigma(t_j)}(t_{j+1}^-, \chi^-(t_{j+1})) = \mu W(t_{j+1}^-) \leq \mu W(t_j). \end{aligned}$$

In the above expressions, the time instant just before t is denoted t^- . When the functions of interest are continuous in t , then $t^- = t$, but we still write t^- instead of t for clarity. In addition, the left limit of a solution $\chi(t)$ at instant t is denoted $\chi^-(t)$. Iterating the last inequality from $j = 0$ to $j = N_\sigma(T, 0) - 1$, we obtain

$$W(T^-) \leq W(t_{N_\sigma(T, 0)}) \leq \mu^{N_\sigma(T, 0)} W(0).$$

Using the definition of W , the above inequality and (20) we have

$$\exp(2\lambda_0 T)V_{\sigma(T^-)}(T, \chi(T)) \leq \exp(2\lambda_0 T^-)V_{\sigma(T^-)}(T^-, \chi(T^-)) \leq \mu^{N_\sigma(T, 0)} V_{\sigma(0)}(0, \chi(0)).$$

Now suppose that σ has the average dwell-time property (5). Hence, we can write

$$\begin{aligned} V_{\sigma(T^-)}(T, \chi(T)) &\leq \exp(-2\lambda_0 T + (N_0 + \frac{T}{\tau_a}) \ln \mu) V_{\sigma(0)}(0, \chi(0)) = \\ &= \exp(N_0 \ln \mu) \exp((\frac{\ln \mu}{\tau_a} - 2\lambda)T) V_{\sigma(0)}(0, \chi(0)). \end{aligned}$$

From the above inequality, we infer that if τ_a satisfies (24), then $V_{\sigma(T^-)}(T, \chi(T))$ converges to zero exponentially as $T \rightarrow \infty$, i.e., it is upper-bounded by $\mu^{N_0} \exp(-2\lambda T) V_{\sigma(0)}(0, \chi(0))$ for some $\lambda \in (0, \lambda_0)$.

Using (21), we obtain $\|\chi(T)\| \leq \sqrt{\frac{c_2}{c_1} \mu^{N_0} \exp(-2\lambda T)} \|\chi(0)\|$. This proves GES.

Notice that the value of the initial time t_0 was fixed to 0 for convenience. In fact, the switched system of interest is GES for any t_0 , i.e., the switched systems is UGES. \square

References

- [1] Poovendran, R: ‘Cyber-physical systems: Close encounters between two worlds [point of view]’, Proceedings of the IEEE, 2010, **98**(8), pp. 1363–1366
- [2] Miorandi, D, Sicari, S, Pellegrini, FD, Chlamtac, I: ‘Internet of things: Vision, applications and research challenges’, Ad Hoc Networks, 2012, **10**(7), pp. 1497–1516
- [3] Ren, W, Beard, RW: Distributed Consensus in Multi-Vehicle Cooperative Control - Theory and Applications, Communications and Control Engineering, (Springer London 2008)
- [4] Akyildiz, IF, Su, W, Sankarasubramanian, Y, Cayirci, E: ‘Wireless sensor networks: a survey’, Computer Networks, March 2002, **38**(4), pp. 393–422
- [5] Kortuem, G, Kawsar, F, Fitton, D, Sundramoorthy, V: ‘Smart objects as building blocks for the internet of things’, Internet Computing, IEEE, 2010, **14**(1), pp. 44–51
- [6] Dimarogonas, DV, Frazzoli, E, Johansson, KH: ‘Distributed event-triggered control for multi-agent systems’, IEEE Trans. on Automatic Control, May 2012, **57**(5), pp. 1291–1297
- [7] Persis, CD, Frasca, P: ‘Robust self-triggered coordination with ternary controllers’, IEEE Trans. on Automatic Control, Dec 2013, **58**(12), pp. 3024–3038
- [8] Yu, H, Antsaklis, PJ: ‘Quantized output synchronization of networked passive systems with event-driven communication’, Proceedings of the American Control Conference (2012), pp. 5706–5711
- [9] Guinaldo, M, Dimarogonas, DV, Johansson, KH, Moreno, JS, Dormido, S: ‘Distributed event-based control strategies for interconnected linear systems’, IET Control Theory & Applications, 2013, **7**(6), pp. 877–886
- [10] Tolić, D: ‘ \mathcal{L}_p -stability with respect to sets applied towards self-triggered communication for single-integrator consensus’, Proc. IEEE Conf. on Decision and Control (2013), pp. 3409–3414
- [11] Persis, CD, Sailer, R, Wirth, F: ‘Parsimonious event-triggered distributed control: A zeno free approach’, Automatica, 2013, **49**(7), pp. 2116 – 2124
- [12] Wang, X, Lemmon, M: ‘Event-triggering in distributed networked control systems’, IEEE Trans. on Automatic Control, 2011, **56**(3), pp. 586–601
- [13] Tolić, D, Fierro, R: ‘Decentralized output synchronization of heterogeneous linear systems with fixed and switching topology via self-triggered communication’, Proc. American Control Conference (2013), pp. 4655–4660

- [14] Raghunathan, V, Schurgers, C, Park, S, Srivastava, M: ‘Energy-aware wireless microsensor networks’, *IEEE Signal Processing Magazine*, 2002, **19**(2), pp. 40–50
- [15] Wei, Y, Heidemann, J, Estrin, D: ‘An energy-efficient mac protocol for wireless sensor networks’, *Twenty-First Annual Joint Conference of the IEEE Computer and Communications Societies INFOCOM*, vol. 3 (2002), pp. 1567–1576
- [16] Le-Huy, P, Roy, S: ‘Low-power wake-up radio for wireless sensor networks’, *Mobile Networks and Applications*, 2010, **15**(2), pp. 226–236
- [17] Tolić, D, Fierro, R, Ferrari, S: ‘Optimal self-triggering for nonlinear systems via approximate dynamic programming’, *IEEE Multi-Conference on Systems and Control* (2012), pp. 879–884
- [18] Williams-II, RL, Lawrence, DA: *Linear State-Space Control Systems*, (John Wiley & Sons2007)
- [19] Bainov, D, Simeonov, P: *Systems with Impulse Effects: Stability, Theory and Applications*, (Ellis Horwood Limited1989)
- [20] Khalil, H: *Nonlinear Systems*, (Prentice Hall2002), 3rd ed.
- [21] Lin, Y, Sontag, ED, Wang, Y: ‘A smooth converse lyapunov theorem for robust stability’, *SIAM Journal on Control and Optimization*, 1996, **34**, pp. 124–160
- [22] Tabbara, M, Nešić, D, Teel, AR: ‘Stability of wireless and wireline networked control systems’, *IEEE Transactions on Automatic Control*, September 2007, **52**(9), pp. 1615–1630
- [23] Liberzon, D: *Switching in Systems and Control*, (Birkhauser Boston2003)
- [24] Hespanha, JP, Morse, AS: ‘Stability of switched systems with average dwell-time’, *IEEE Conference on Decision and Control* (1999), pp. 2655–2660
- [25] Goebel, R, Sanfelice, RG, Teel, AR: ‘Hybrid dynamical systems’, *IEEE Control Sys. Magazine*, 2009, **29**(2), pp. 28 – 93
- [26] Schmid, T, Charbiwala, Z, Friedman, J, Cho, YH, Srivastava, MB: ‘Exploiting manufacturing variations for compensating environment-induced clock drift in time synchronization’, *Proc. ACM International conference on Measurement and modeling of computer systems (SIGMETRICS)* (2008), pp. 97–108
- [27] Bao, L, Garcia-Luna-Acaves, J: ‘Link-state routing in networks with unidirectional links’, *Eight International Conference in Computer Communications and Networks* (1999), pp. 358–363

- [28] Tolić, D, Sanfelice, RG, Fierro, R: ‘Input-output triggered control via the small gain theorem and switched systems modeling’, *International Journal of Robust and Nonlinear Control*, to appear
- [29] Nowzari, C, Cortés, J: ‘Team-triggered coordination of networked systems’, *Proceedings of the American Control Conference (2013)*, pp. 3827–3832
- [30] Rugh, WJ: *Linear System Theory*, (Prentice Hall, Englewood Cliffs, NJ1996), 2nd ed.
- [31] Tolić, D, Hirche, S: ‘Stabilizing transmission intervals and delays for linear time-varying control systems: The large delay case’, *20th Mediterranean Conference on Control and Automation (2014)*, to appear
- [32] Kingston, DB, , Ren, W, Beard, RW: ‘Consensus algorithms are input-to-state stable’, *Proceedings of the American Control Conference (2005)*, pp. 1686–1690
- [33] Jeličić, V, Tolić, D, Bilas, V: ‘Consensus-based decentralized resource sharing between co-located wireless sensor networks’, *IEEE Ninth International Conference on Intelligent Sensors, Sensor Networks and Information Processing (ISSNIP) (2014)*
- [34] Kwon, WH, Moon, YS, Ahn, SC: ‘Bounds in algebraic riccati and lyapunov equations: A survey and some new results’, *International Journal of Control*, 1996, **64**(3), pp. 377–389
- [35] Bhatia, R: *Matrix Analysis*, (Springer-Verlag New York, Inc., New York, NY1997)
- [36] Piazza, G, Politi, T: ‘An upper bound for the condition number of a matrix in spectral norm’, *Journal of Computational and Appl. Math.*, 2002, **143**(1), pp. 141–144
- [37] Jeličić, V, Magno, M, Brunelli, D, Bilas, V, Benini, L: ‘An energy efficient multimodal wireless video sensor networkwith eZ430-RF2500 modules’, *Proc. 5th Internat. Conf. on Pervasive Computing and Appl. (ICPCA) (2010)*, pp. 161–166
- [38] Texas Instruments: *eZ430-RF2500 Development Tool User’s Guide*, 2009
- [39] Dilmaghani, RS, Bobarshad, H, Ghavami, M, Choobkar, S, Wolfe, C: ‘Wireless sensor networks for monitoring physiological signals of multiple patients’, *IEEE Trans. on biomedical circuits and systems*, Aug. 2011, **5**(4), pp. 347–356
- [40] Franceschelli, M, Gasparri, A, Giua, A, Ulivi, G: ‘Decentralized stabilization of heterogeneous linear multi-agent systems’, *IEEE Int. Conf. on Robotics and Automation (2010)*, pp. 3556–3561
- [41] Bartle, RG: *The Elements of Integration and Lebesgue Measure*, (Wiley-Interscience1995), 1st ed.